ATOMIC STRUCTURE OF TRANSITION METAL BASED METALLIC GLASSES

Thesis by

Arthur Williams

In Partial Fulfillment of the Requirements

for the Degree of

Doctor of Philosophy

California Institute of Technology

Pasadena, California

1981

(Submitted January 5, 1981)

To Sandy

ACKNOWLEDGEMENTS

I would like to acknowledge the patient support of Professor William Johnson and Professor Pol Duwez for providing the opportunity to perform this research and for introducing me to the exciting field of amorphous metals. I am particularly grateful for the advice and encouragement given me by Professor Johnson, and it is a great privilege for me to have become his first student.

For technical assistance, and for their friendship, I would like to thank Concetto Geremia, Joe Wysocki and Angela Bressan. I would especially like to thank Mr. Sumio Kotake, whose absence from the lab for the past year has been deeply felt. It is the sincerest wish of the entire group at Keck Lab that he will recover quickly and soon be able to return to the group. It is my hope that many more students will have the benefit of both his expertise and friendship, as I have.

For typing the manuscript I would like to thank Beth McGrath and Linda Malaby.

Financial support from the United States Department of Energy and from the International Business Machine Corporation are gratefully appreciated.

ABSTRACT

The atomic-scale structure of several transition metal-based metallic glasses has been investigated by X-ray diffraction techniques. Current dense random packing models have been found to have only a superficial resemblance to the structure of real amorphous metallic alloys, and a theoretical density for amorphous transition metals has been obtained which might be used as a filter for more realistic single component models in the future. The partial pair distribution functions for individual pairs of atomic species have been obtained for glassy alloys of lanthanum with aluminum, gallium and gold through the use of isomorphous alloys. These systems have been demonstrated to be chemically ordered and the short range order of these alloys has been shown to be quite different from that of typical amorphous transition metal-metalloid alloys.

TABLE OF CONTENTS

LIST OF TABLES

LIST OF FIGURES

I. INTRODUCTION

The structure of metallic glasses has received considerable attention since the observation in 1960 of a broad diffuse band in the X-ray diffraction pattern of gold-silicon alloys rapidly quenched from the liquid melt. [1] In these early experiments Duwez et al. [2] found that by forcing a droplet of molten alloy at close to the speed of sound against a copper substrate, (the "gun" technique), the subsequent cooling rate of about 10^6 degrees C per second was sufficient to quench some transition metal-metalloid alloys of near eutectic composition into an amorphous phase. A similar quench rate was later achieved by the "piston and anvil" method by catching a falling droplet of molten alloy between two rapidly moving copper plates, [3] a technique which had the advantage of producing more useful samples in the form of foils about 40 microns thick and one centimeter in diameter. Improved techniques have since been developed so that now many glassy metals can be produced commercially in the form of continuous ribbons as much as several inches wide by squirting a stream of molten alloy onto a rapidly rotating metal wheel. [4]

Since the early work of Duwez et al. [1, 5, 6] it has been found that a large number of metallic alloy systems can be quenched amorphous from the liquid state at compositions near a deep eutectic in the phase diagram for the constituents. No crystalline diffraction peaks are observed for the amorphous solid but rather only a single diffuse primary band followed by a series of smaller maxima. To date the majority of metallic glasses which have been produced have been alloys of transition metals with one or more of the nonmetallic (metalloid) elements of

valence 3, 4 or 5 such as B, C, Si and P. Such alloys as Pd-Si, Fe-B, and Pd-Cu-P are therefore often referred to as transition metal-metalloid (TM-M) alloys. The composition at which these systems can be quenched into glassy metals is typically at about 20 atomic percent of the metalloid, which is always associated with a low melting point eutectic in the phase diagram of the constituents. Some systems of early transition metal-late transition metal alloys such as Zr-Cu, Nb-Ni and Y-Fe can also be quenched amorphous near their eutectics, as can some rare earth-transition metal alloys such as Gd-Co and even some simple metal alloys such as Pb-Au.

To date, the bulk of experimental investigations of the atomic scale structure of metallic glasses, (i.e., metallic alloys quenched amorphous from the liquid melt), has been the result of X-ray diffraction experiments. Electron diffraction techniques have been used to study vapor quenched thin films of amorphous metals and alloys [7] but have not been applied to bulk glassy metals. Only a very thin layer of the surface would be observable in any case due to the short mean free path (tens of Angstroms) of electrons in metals, and oxidation, gas inclusions and other surface irregularities may make such an observation unrepresentative of the bulk material. Neutron diffraction experiments suffer from the opposite problem of a very long mean free path (millimeters) for neutrons in the material. Relatively large (several grams) samples are therefore necessary and were generally unavailable, limiting early experiments for the most part to materials which could be electrolitically deposited in an amorphous state in bulk form such as Co-P. [8] With the development of reliable methods of producing long

ribbons of high quality metallic glasses however, neutron diffraction experiments are becoming more popular.

The recent availability of synchrotron radiation sources and the rapid development of extended X-ray absorption fine structure techniques has inspired the use of EXAFS to study a few metallic glasses. [9] A powerful advantage of this technique is the capability of tuning in on a particular atomic specie, allowing the acquisition of more specialized information than is generally available from diffraction experiments. The lack of low K information however, as well as other considerations may limit the usefulness of EXAFS studies for very disordered systems. [10]

A typical experimental arrangement for X-ray diffraction as shown in figure (1) measures the intensity profile of radiation of some known energy scattering from a sample as a function of the momentum transfer K. For elastic (Rayleigh) scattering the momentum transfer is given by $K = \frac{4\pi}{\lambda} \sin\theta$ where 2θ is the scattering angle and λ is the wavelength of the incident (and elastically scattered) radiation. Since electrons are the fundamental scatterers of X-rays (and electrons), the ratio of intensities of scattered to incident radiation is usually expressed in terms of the scattering power of a single free Thompson electron, called an electron unit (e.u.). The ratio of scattered to incident amplitudes for a single free atom is called the atomic form factor $f(k)$, the squared modulus of which is equal at $K=0$ to the square of the atomic number Z in electron units. For $K>0$, $|f(k)|^2$ monotonically decreases due to the interference effects among the individual electrons, a result of the fact that the dimensions of the spatial distribution of

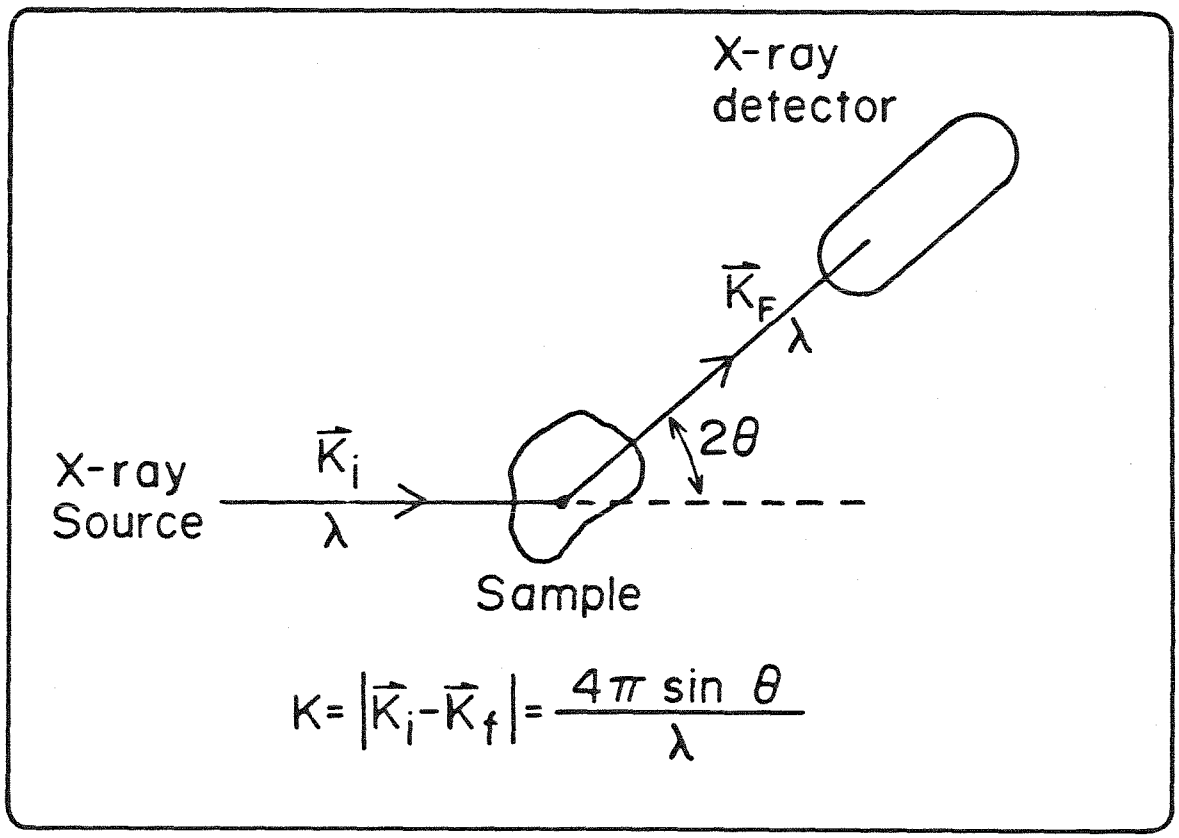

Figure 1. Elastic scattering of X-rays with wavelength λ through an angle 2θ.

the atomic electrons is of the same order of magnitude as the X-ray wavelengths (0.5 Å to 1.5 Å). For the case of neutron scattering, where it is the nucleus rather than the electrons which do the scattering, the analogous nuclear scattering lengths, b, are independent of K due to the relatively very small nuclear dimensions. This fact simplifies some aspects of the interpretation of data acquired by neutron experiments.

The total intensity of elastically scattered radiation from a homogeneous isotropic substance containing n different atomic species and N atoms is the squared modulus of the total amplitude and is given by the well known [11-15] expression

$$I_n(K) = N\left[\sum_{i=1}^{n} C_i\,|f_i(K)|^2 + \frac{1}{K}\sum_{i=1}^{n}\sum_{j=1}^{n} C_iC_jf_i(K)f_j^*(K)\int_0^\infty 4\pi r\,(\rho_{ij}(r)/C_j - \rho_0)\sin(Kr)dr\right] \quad (1)$$

where C_i and f_i are the fractional concentration and atomic form factor of element i and ρ_0 is the bulk atomic density of the material. The function $\rho_{ij}(r)$ is the average atomic density of j type atoms a distance r away from an i type atom averaged over all the i atoms in the material. The quantity $4\pi r\,(\rho_{ij}(r)/C_j - \rho_0)$ is sometimes called the reduced radial pair distribution function, $G_{ij}(r)$. The diffraction intensity profile can therefore provide direct information on the structure of a material in the form of probability distribution functions between pairs of atoms, yielding information on inter-atomic distances and coordination numbers. It is immediately obvious, however, that extraction of the real space functions $\rho_{ij}(r)$ is not simple when

the f_i are functions of K. Hence it is common practice in X-ray analysis to define the interference function I(K) as

$$I(K) = 1 + \frac{I_n(K) - N\langle|f(K)|^2\rangle}{|\langle f(K)\rangle|^2} \qquad (2)$$

$$= 1 + \frac{1}{K}\sum_{i,j} W_{ij}(K)\int_0^\infty 4\pi r(\rho_{ij}(r)/C_j - \rho_0)\sin(Kr)dr$$

where $\langle\ \rangle$ represents a compositional average and $W_{ij}(K) = C_iC_j \frac{f_i(K)f_j^*(K)}{|\langle f(K)\rangle|^2}$. The $W_{ij}(K)$ appearing in the double sum now are much more slowly varying functions of K than the $f_i(K)$ as can be seen in figure (2) for $Pd_{80}Si_{20}$. This allows the simplifying Warren-Krutter-Morningstar,[12] or WKM approximation, $W_{ij}(K)$ = constant, to be made which makes possible the inverse sine transform of equation (2) as

$$G(r) = 4\pi r \sum_{i,j} W_{ij}\ (\rho_{ij}(r)/C_j - \rho_0) \qquad (3)$$

$$\simeq \frac{2}{\pi}\int_0^\infty K(I(K) - 1)\sin(Kr)dK$$

The function G(r) is therefore a linear combination of the n^2 individual pair density functions, with weighting approximately proportional to $C_iC_jZ_iZ_j$, the product of concentrations and atomic numbers. For multiconstituent systems this averaging can severely limit the amount of information which can be extracted from a simple diffraction experiment. Fortunately a large number of TM-M alloys

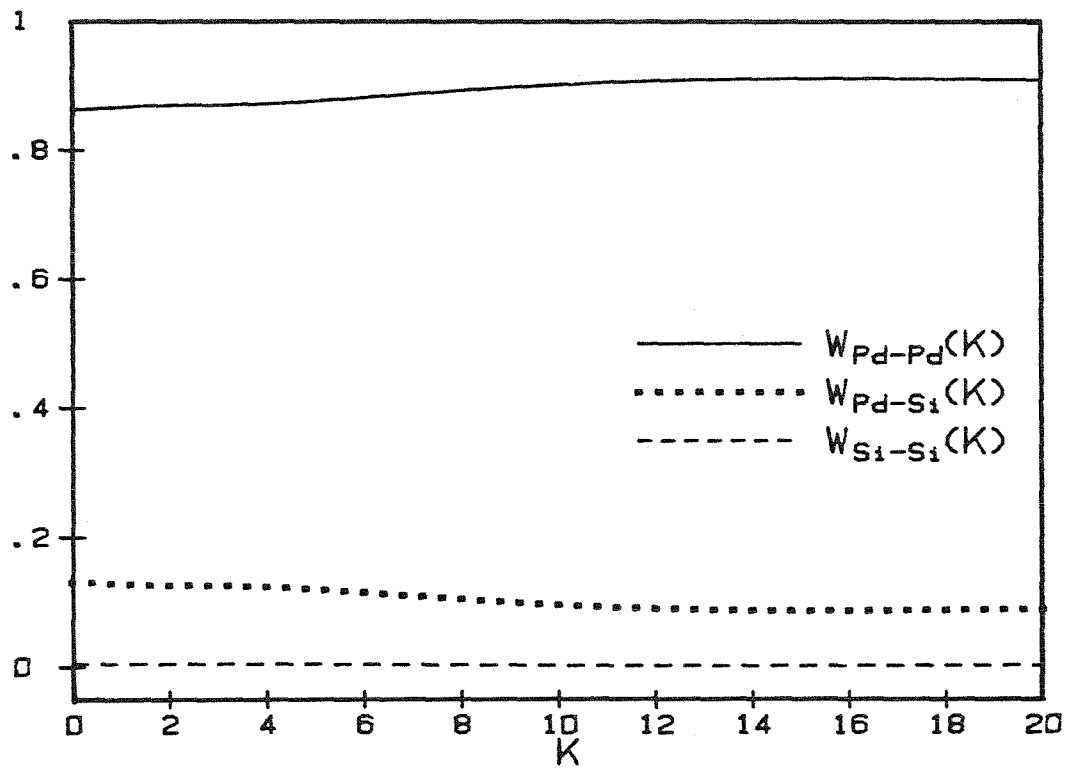

Figure 2. X-ray scattering coefficients, $W_{ij}(K)$ for $Pd_{80}Si_{20}$.

which can be made amorphous weight primarily the transition metal-transition metal pairs due to the relatively smaller atomic number and concentration of the metalloid constituents. This helps simplify somewhat the interpretation of X-ray scattering results for the TM-M alloy systems. For the metallic glass $Pd_{80}Si_{20}$, for example, scattering by pairs of transition metal atoms is responsible for more than 90% of the X-ray interference function shown in figure (2). Figure (2) of the weighting functions $W_{ij}(K)$ also shows that most of the remaining 10% is the result of Pd-Si scattering with Si-Si scattering accounting for less than one percent of the total.

Comparison of the I(K) and G(r) for glassy $Pd_{80}Si_{20}$ to those of the liquid transition metal (figures (3) and (4)) show sharper and more extended features for the metallic glass, suggesting that considerably more short range order exists in the amorphous metallic alloy than in the liquid metal. The split second band in G(r) is a very common feature of amorphous TM-M alloys, as is the shoulder on the high K side of the second maximum of I(K). Neither is observed in liquid metals. The density of the glassy alloys is higher than for the liquid alloy, being typically only one or two percent lower than that of the corresponding crystalline phase. This high density coupled with lack of long range order make it unclear whether amorphous metals should be more properly related to disordered crystalline solids or to liquid metals. Models for glassy metals can therefore be grouped generally into those which assume a large number of very small (tens of atoms) randomly oriented crystals and those which assume a homogeneous random packing without structural discontinuities.

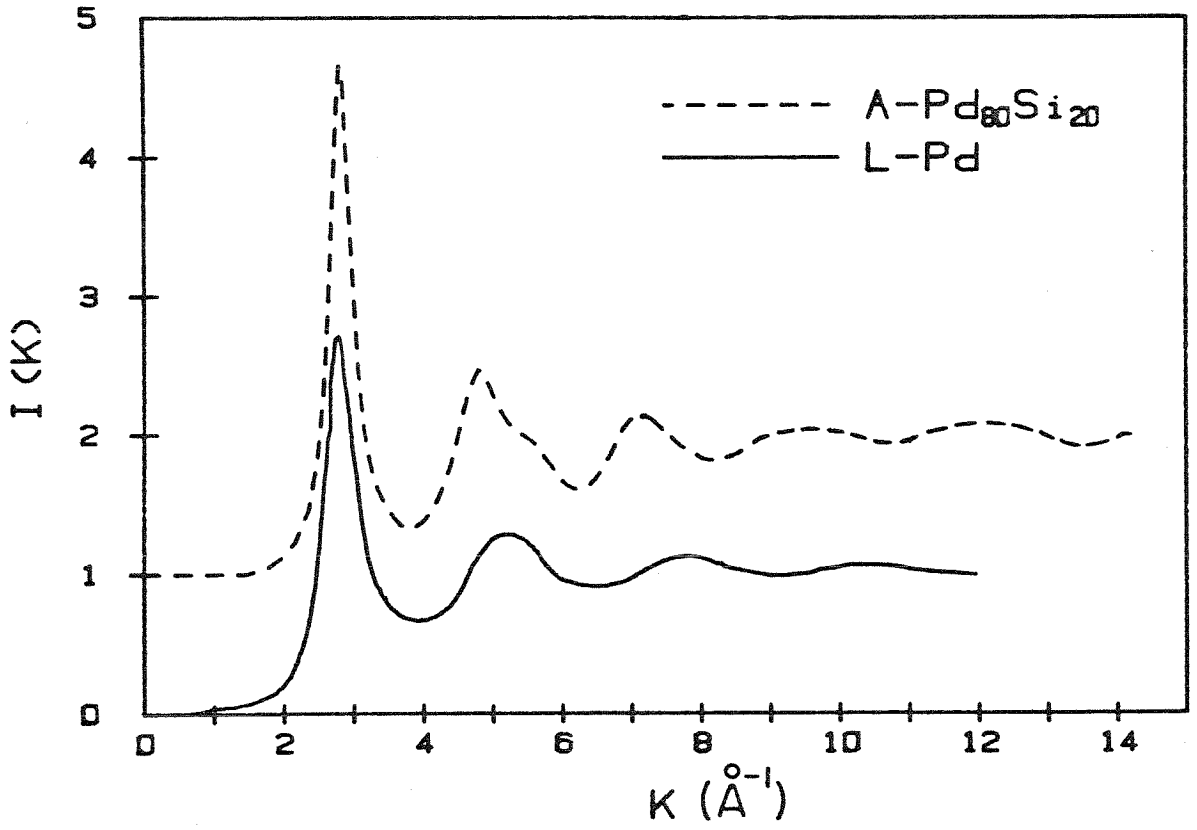

Figure 3. X-ray interference functions, I(K), for $Pd_{80}Si_{20}$ metallic glass [R. C. Crewdson, Ph.D. thesis, Calif. Inst. of Tech., Pasadena, CA, 1966] and liquid Pd [Y. Waseda and M. Ohtani, Z. Physik B 21, 229 (1975)].

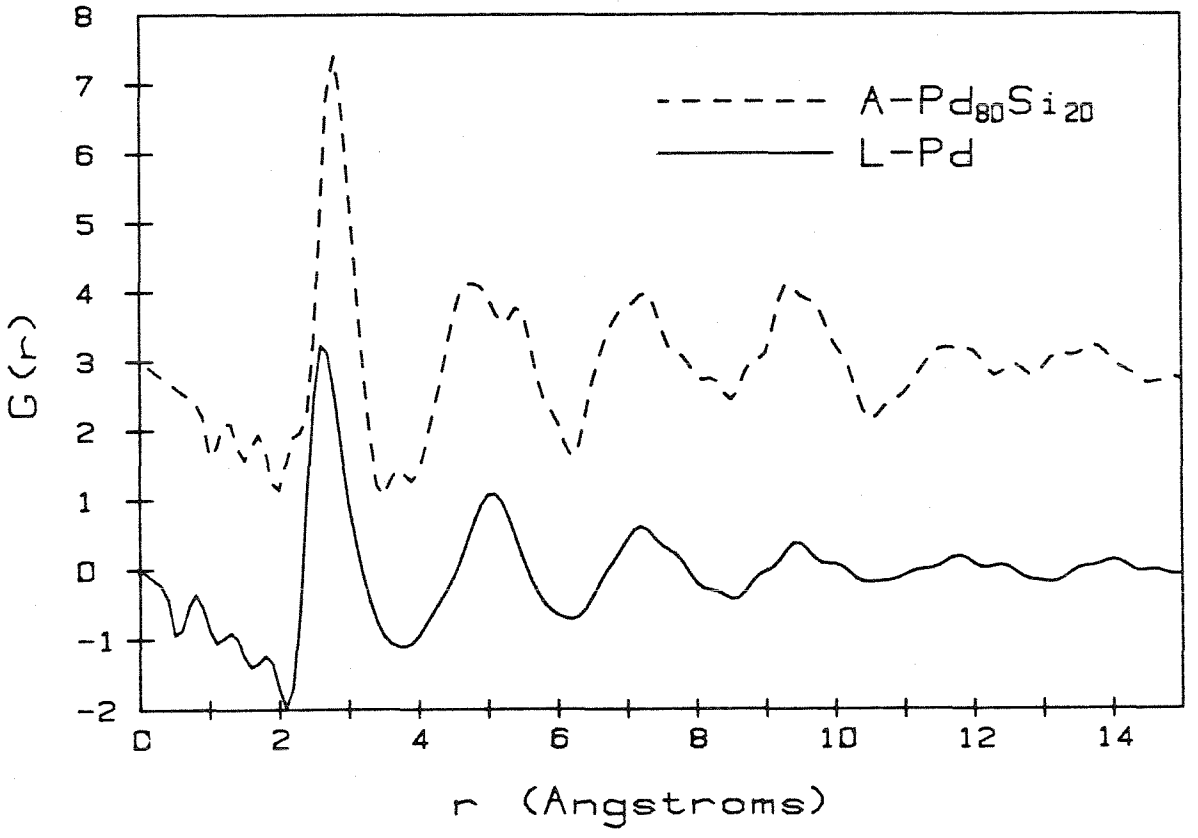

Figure 4. Reduced radial distribution functions, G(r), for $Pd_{80}Si_{20}$ metallic glass and liquid Pd calculated from the interference functions in figure 3.

Microcrystalline models are lent support by the fact that many metallic glasses exhibit prominent diffraction maxima near the Bragg peaks in the corresponding crystalline compounds. Broadening of the crystalline Bragg reflections can occur from small crystal sizes, inhomogeneous strains and stacking faults. [16] For comparison with amorphous metals, a model intensity function can be computed from the Debye equation

$$I_N(K) = N \sum_{ij}^{n} f_i(K) f_j^*(K) \frac{\sin(K r_{ij})}{K r_{ij}}$$

for scattering from N identical randomly oriented crystals containing n atoms where $\bar{r}_{ij}$ is the vector between atoms i and j. [17-21] Figure (5) shows the microcrystalline I(K) for FCC microcrystals with 125 atoms each and a = 3.90 Å and a Debye Waller damping term $e^{-\langle u^2 \rangle K^2}$ with $\langle u^2 \rangle = .01$ Å^3. [22] Also shown are two experimental interference functions for two 10,000 Å films of Ag-Cu alloys with similar compositions. [21, 23] The film deposited on vitreous silica is microcrystalline while the film deposited on beryllium, which is a better thermal conductor, is not. Microcrystalline models have had little real success in reproducing the structural characteristics of most amorphous metal alloys.

Somewhat more successful models for the structure of metallic glasses have been based on the Bernal picture of the dense random packing of hard spheres (DRPHS), a model first proposed for the structure of noble gas liquids. [24-26] The original investigations of Bernal and his students involved collecting steel ball bearings in rubber bladders which were then kneaded to optimize the packing

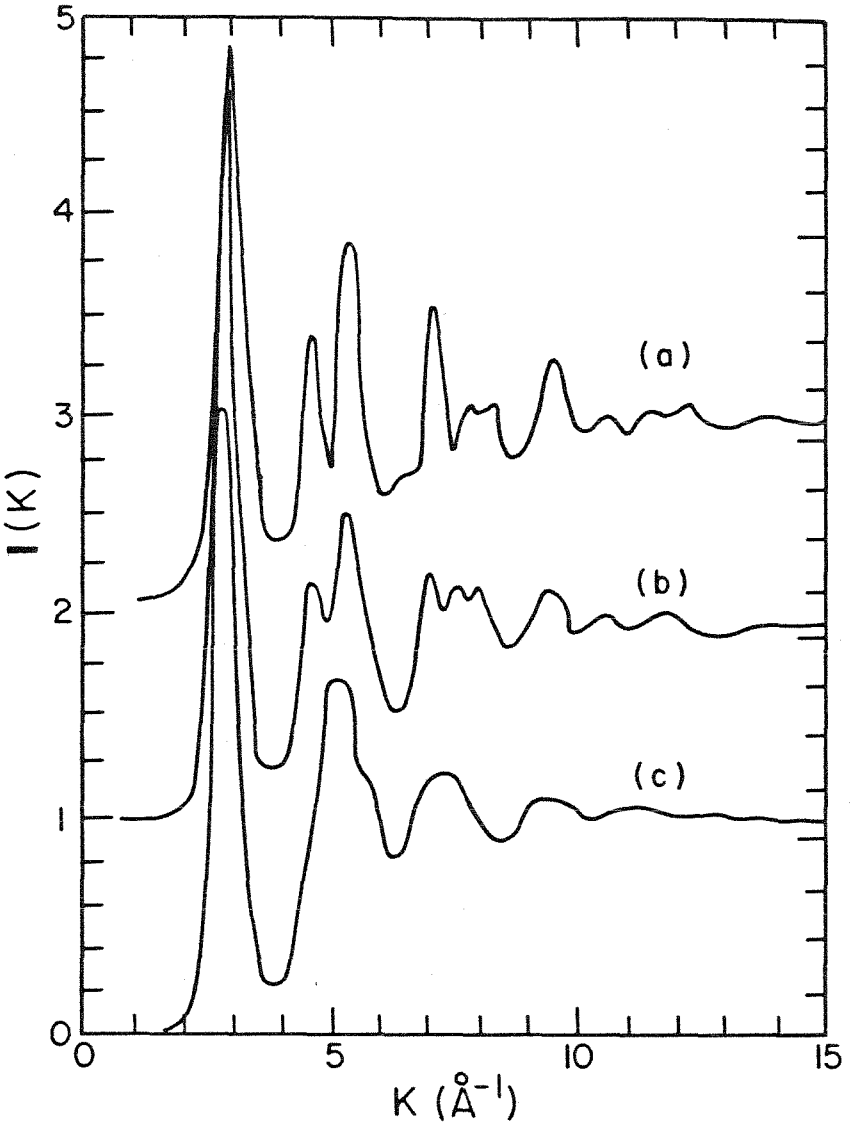

Figure 5. Interference functions I(K): a) calculated for FCC microcrystals with 125 atoms and $\langle u^2 \rangle$ = 0.01 Å^2 [C. N. J. Wagner, T. B. Light, N. C. Halder, and W. E. Lukens, J. Appl. Phys. 39, 3690 (1968)]; b) obtained experimentally for a 10,000 Å film of $Ag_{48}Cu_{52}$ deposited on a vitreous silica substrate at 77° K [ibid]; c) obtained experimentally for a similarly prepared film of $Ag_{55}Cu_{45}$ deposited on a beryllium substrate in a poorer vacuum [W. E. Lukens, Ph.D. Thesis, Yale University, New Haven, Conn. 1971].

density. The model was fixed by pouring in black paint and allowing it to dry and then the ball positions were measured with a mechanical device. The most ambitious project of this sort was carried out by Finney[27] on a dense random packing of 7994 spheres. The distribution function $g(r) = \rho(r)/\rho_0$ for this model in the form of a histogram is shown in figure (6) along with a similar model by Scott and Kilgour[28] using only 1000 balls. The packing fractions for both models were determined independently to be 0.6366, which is 10 to 20% smaller than for metallic glasses, but the shape of the model distribution functions reproduces reasonably well most of the features of those of amorphous TM-M alloys.

The reduced radial distribution function $G(r) = 4\pi r\,(\rho(r) - \rho_0)$ for the Bernal-Finney model is plotted in figure (7) with that obtained by Cargill [22] for amorphous $Ni_{76}P_{24}$. The only adjustable parameter is the hard sphere radius which was taken by Cargill to be 1.23 Å in order to get the best fit for the data. This is slightly smaller than the nickel Goldschmidt radius, but since Ni-P correlations are responsible for about 14% of the X-ray scattering in $Ni_{76}P_{24}$ this is not unreasonable. The abrupt drops in the G(r) histogram at r = 1 and r = 2 (sphere diameters) are natural consequences of the hard sphere nature of the interatomic potential used. The hard sphere configurations which produce the splitting in the second maximum of G(r) have been discussed by Finney [29] and Bennett [30] and are illustrated in figure (8). In the DRPHS model the maxima are at 1.73 and 1.99 hard sphere diameters, which correspond respectively to opposite apices of two tetrahedra which share a common side and to three nearly collinear

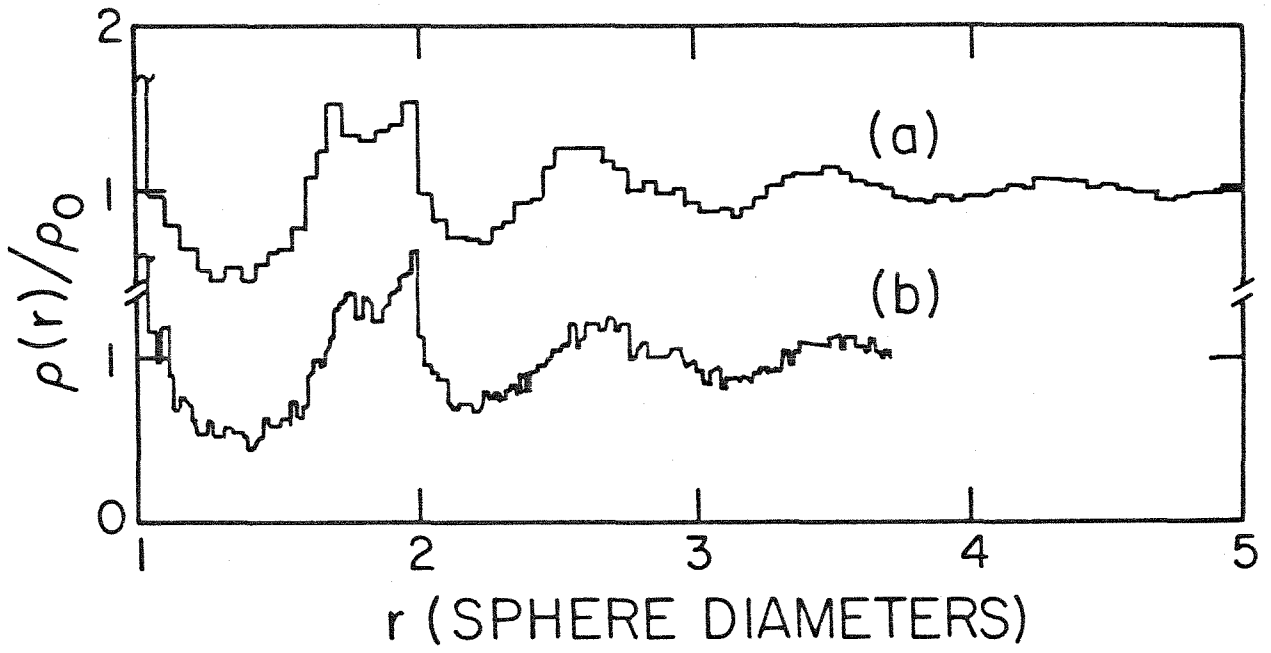

Figure 6. Distribution function $g(r) = \rho(r)/\rho_0$ for DRPHS of single sized ball bearings: a) for 7994 sphere model of J. L. Finney [Proc. Roy. Soc., Ser. A 319, 495 (1970)]; b) for 1000 ball model of Scott [Nature (London) 194, 956 (1962)] taken from D. J. Adams and A. J. Matheson, J. Chem. Phys. 56, 1989 (1972).

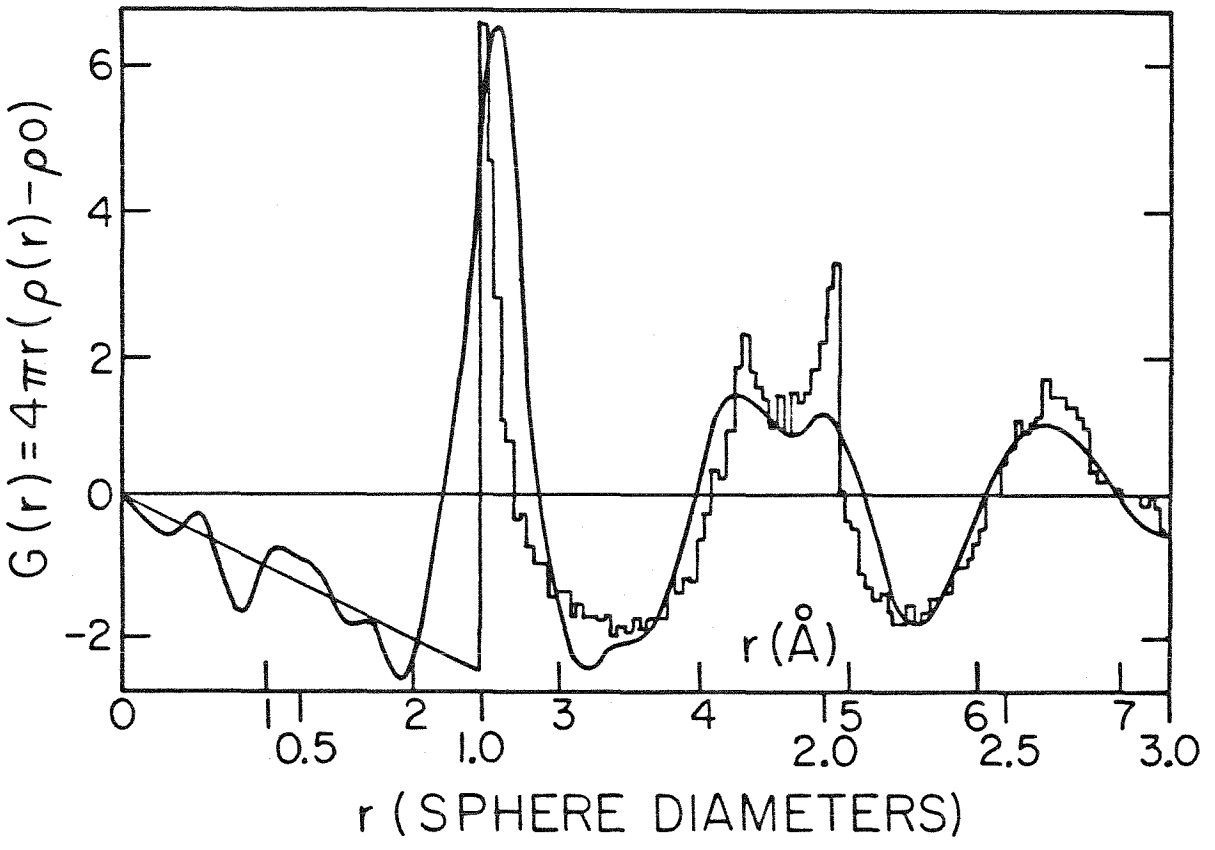

Figure 7. Comparison of reduced radial distribution functions, $G(r) = 4\pi r\,[\rho(r)-\rho_0]$, for Finney's DRPHS model (histogram) and for electrodeposited amorphous $Ni_{76}P_{24}$ [G. S. Cargill III, J. Appl. Phys. 41, 12 (1970)].

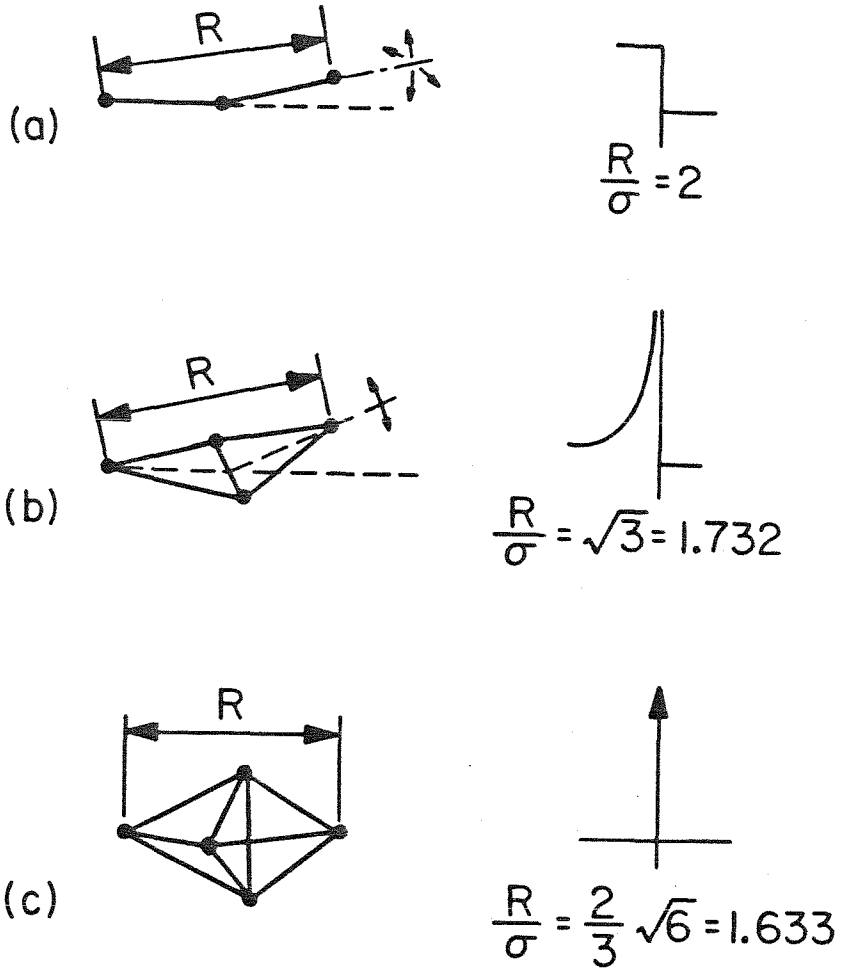

Figure 8. Simple connected groups of particles and their discontinuous contributions to the pair distribution function. Two darkened circles connected by a solid line denote two particles in hard contact and D_{HS} is the hard sphere diameter [C. H. Bennett, J. Appl. Phys. 43, 2727 (1972)].

spheres. Bernal showed that the maximum density DRPHS is 70% composed of perfect tetrahedra which are organized into dense collections of long twisted spirals which he called pseudonuclei, [26] and in which these configurations occur very frequently. The peak at 1.99 is also seen in most amorphous TM-M alloys; however,the first subpeak in the second band is more often closer to 1.63. This represents the separation of opposing apices of two tetrahedra sharing a common base as in figure (8c). More refined, computer generated models of relaxed hard sphere packings and binary packings using spheres with two different radii have had little success in generating distribution functions with peaks at this characteristic distance although they have been able to correctly reproduce the relative heights of the first and second peak in the second band. [31-33]

The packing fractions and atomic densities of the DRPHS models are 10 to 20% lower than for amorphous metals. Polk [34] has suggested that for TM-M systems the DRPHS matrix of transition metal atoms occurs for these amorphous alloys with the smaller metalloid atoms occupying the larger holes in the structure. The type and frequency of occurrence of the holes which occur in a DRPHS has been determined by Bernal, [26] and Cargill and Cochrane[35] have pointed out that these Bernal holes are too small to accommodate the metalloid atoms. Polk has therefore suggested that a local rearrangement of the transition metal matrix can occur in the neighborhood of the holes in order to accommodate the metalloid atoms. [36] The occurrence of such interstitial atoms in the structure would be expected to result in a correspondingly higher atomic density than for the pure DRPHS matrix. Binary hard

sphere packing models, computer relaxed models and molecular dynamics calculations have been able to improve on the packing density of the Bernal DRPHS by a few percent only, leaving still a large gap between the model densities and those observed for amorphous metal alloys. (31-33, 37-39)

X-ray studies of amorphous metal-metal alloys have usually been complicated by the fact that both constituents make substantial contributions to the scattering, which results in a total G(r) which is an approximate linear combination of a number of pair distribution functions. The I(K) and G(r) of many early transition metal-late transition metal amorphous alloys are much more featureless than those of TM-M systems. Correlations beyond the main peak are also apparently much weaker in rare earth-transition metal alloys in which small atoms (TM) are compositionally dominant (67-82%), and Cargill has suggested that in binary alloys of this type, (e.g., Gd-Co, Gd-Fe, Tb-Fe), the three partial pair distribution functions may cancel one another when combined in the experimentally accessible distribution functions. (40) The usefulness of DRPHS structural models has not yet been demonstrated for amorphous metal-metal alloys.

The individual pair density functions that appear in equation (2) can sometimes be recovered if sufficient information can be obtained. Since, for an isotropic material, $\rho_{ij}(r)/C_j = \rho_{ji}(r)/C_i$ there are $\frac{1}{2}n(n+1)$ independent pair density functions for an n constituent alloy. For a binary alloy then, there are only three independent pair correlation functions, and since equation (2) is linear the availability of three independent I(K) with known $W_{ij}(K)$ makes possible their solution. Unfortunately it is not always possible to perform three

diffraction experiments with sufficiently different $W_{ij}(K)$ to allow equation (2) to be solved with any accuracy. The first experiments to do so were done by Enderby et al. [41] who performed neutron diffraction experiments on three liquid Cu-Sn alloys using three different nuclear isotopes of Cu which have different neutron scattering lengths.

The three partial pair distribution functions have been reliably determined in the past for only a very few binary metallic glasses. Sadoc and Dixmier [42] made the first study of an amorphous metal using combined unpolarized neutron, polarized neutron, and X-ray diffraction data to determine $G_{Co-Co}(r)$, $G_{Co-P}(r)$, and $G_{P-P}(r)$ for a ferromagnetic Co-P alloy. They found no P-P near neighbors in the alloy and concluded that these metalloid atoms occupy holes in the structure as suggested by Polk. Mizoguchi et al. [43] used time-of-flight neutron diffraction and three nuclear isotopes of Cu to study glassy $Zr_{43}Cu_{57}$ and found all nearest neighbor distances to be approximately equal to the sum of the metallic radii of the two atoms, and that all three $G_{ij}(r)$ exhibit assymmetric second maxima. They concluded that, quite unlike the amorphous TM-M alloys, no chemical short range order exists in this early transition metal-late transition metal glass. Waseda and Chen[44] have attempted to use the anomalous dispersion of X-rays near the K-absorption edges of the constituent elements of metallic glasses of Zr and some 3d late transition metals to obtain partial pair distribution functions. This technique takes advantage of the change in the atomic form factor $f = f_o + \Delta f'(\omega) + i\Delta f''(\omega)$ for energies near an X-ray absorption edge of the atom. The changes are small and poorly known, however, at the energies available

to Waseda's group using conventional X-ray sources, and the errors in the resulting distribution functions are likely to be very large. Very recent work using the tunable high intensity X-ray radiation available from synchrotron sources, however, suggests that the anomalous dispersion approach may become very attractive in the future as a tool for studying disordered materials. [45] Another approach, suggested by Chipman et al. [46], is that of isomorphous substitution, in which chemically similar elements such as Zr and Hf, or Mo and W, are substituted for each other in an amorphous alloy which might then be assumed to be isostructural to its counterpart. Thus, for example, if glassy $Zr_{40}Cu_{60}$, $(Zr_{0.5}Hf_{0.5})_{40}Cu_{60}$, and $Hf_{40}Cu_{60}$ are isostructural then the three interference functions that can be obtained are sufficient to obtain the three partial pair correlation functions. This technique is only applicable of course to a few, well chosen systems of alloys and its use with metallic glasses up until now, except for the above mentioned system, has not been reported, although Cargill has obtained approximate partial radial distribution functions for Nb-Nb and Nb-Si pairs using data from presumably isomorphous thin films of amorphous Nb_3Si and Nb_3Ge [47] and by ignoring the small Si-Si, (and Ge-Ge), contributions to the I(K)s.

In this study the I(K) and G(r) of several metallic glasses are computed from X-ray diffraction data and compared to DRPHS and similar models. The first group of alloys considered are ternary and quarternary, (although sometimes referred to as pseudobinary), TM-M type metallic glasses based on refractory transition metals. It is unfortunate that no true binary alloys of this nature have been found to be conveniently quenchable into a glassy state, but considerable work has

been done recently on Mo-Ru, Mo-Re, and W-Ru based glasses, [48-50] including characterization of electronic, mechanical, and superconducting properties. Tungsten-ruthenium based alloys are chosen for the diffraction study since the relatively large atomic numbers of these refractory transition metals minimizes the effective scattering contributions from the metalloid atoms. The total G(r) is then representative of the transition metal atoms and is computed for each alloy and found to have striking qualitative similarity to the Bernal-Finney model for hard spheres but much less impressive quantitative agreement. Approximate transition metal coordination numbers are obtained by varying the metalloid specie of the alloy and density measurements of chemically similar Mo-Ru based metallic glasses, as well as a large number of other TM-M alloys are analyzed as functions of metalloid content.

The second group of metallic glasses considered are La based alloys of Al, Ga, and Au. The short range order of these metallic glasses is quite different from amorphous TM-M alloys and the computed G(r)s have more resemblance to those of liquid metals than to the DRPHS. Considerable evidence for chemical ordering is found to exist for these alloys, which is especially conspicuous for $La_{1-x}Au_x$ glasses, which exhibit a distinct prepeak in the X-ray diffraction profile. The three partial pair density functions, (e.g., $\rho_{La-La}(r)$, $\rho_{La-Au}(r)$ $\rho_{Au-Au}(r)$), for the binary La alloys is determined by isomorphous substitution of elements, and the most probable interatomic distances and atomic coordination numbers are determined and compared to the corresponding crystalline intermetallic compound and to previous results on amorphous TM-M alloys.

II. EXPERIMENTAL PROCEDURES

Alloys were prepared by rf levitation melting of appropriate constituents under an argon atmosphere on a water cooled silver boat. Ingots were remelted several times and then broken apart and visually inspected for homogeneity. Purity and character of the elements used in this study were as follows:

Al	rod	99.995%
Au	powder	99.99 %
B	lump	99.9 %
Ga	bulk	99.999%
La	rod	99.9 %
Mo	rod	99.99 %
P	red amorphous powder	technical
Ru	-10 mesh sponge	99.98 %
Si	bulk	99.99 %
W	rod	99.993%

The alloys that were prepared for X-ray diffraction experiments are listed in Table I. Because of the very high vapor pressure of elemental phosphorus it was necessary to sinter a powder compact of the $W_{40}Ru_{40}P_{20}$ alloy in a sealed quartz tube prior to melting as above.

Due to the low melting points and high solubilities in silver of aluminum and gallium, the pure metals were never allowed to come in contact with the silver levitation boat, but rather were placed in pits drilled out of the lanthanum with which they were to be alloyed. The bulk lanthanum was first cleaned by sealing under vacuum in one end of

$(TM)_{1-x}M_x$ Alloy*	W_{TM-TM}	$(W_{TM-M} + W_{M-TM})$	W_{M-M}
$(W_{0.5}Ru_{0.5})_{80}B_{20}$	0.9589	0.0406	0.0004
$(W_{0.5}Ru_{0.5})_{80}B_{10}Al_{10}$	0.9279	0.0708	0.0013
$(W_{0.5}Ru_{0.5})_{80}B_{10}Si_{10}$	0.9241	0.0744	0.0015
$(W_{0.5}Ru_{0.5})_{80}P_{20}$	0.8840	0.1124	0.0036
$La_{80}Al_{20}$	0.8950	0.1021	0.0029
$La_{80}Al_{10}Ga_{10}$	0.8317	0.1605	0.0077
$La_{80}Ga_{20}$	0.7749	0.2107	0.0143
$La_{80}Au_{20}$	0.5516	0.3822	0.0662
$La_{76}Al_{24}$	0.8701	0.1253	0.0045
$La_{76}Al_{12}Ga_{12}$	0.7945	0.1937	0.0118
$La_{76}Ga_{24}$	0.7283	0.2502	0.0215
$La_{76}Au_{24}$	0.4838	0.4235	0.0927
$La_{72}Al_{28}$	0.8437	0.1497	0.0066
$La_{72}Al_{14}Ga_{14}$	0.7560	0.2270	0.0170
$La_{72}Ga_{28}$	0.6813	0.2882	0.0305
$La_{72}Au_{28}$	0.4222	0.4551	0.1227

*TM = transition metal

* M = metalloids

Table I. X-ray scattering weights of individual pairs of atomic species of the alloys studied.

a quartz tube containing some strips of pure titanium. The titanium was heated in one end of the tube to about 850 C and allowed to getter while the lanthanum in the other end was heated to 500 C and allowed to outgas. The titanium was allowed to getter in this manner for several days during which time the lanthanum became visibly much cleaner.

Amorphous samples in the form of foils about 40 microns thick and typically 1 to 2 centimeters in diameter were obtained by rapidly quenching from the liquid melt by the piston and anvil technique [3] under a helium atmosphere. All foils obtained in this way were first checked for crystalline inclusions on a Norelco scanning X-ray diffractometer using copper $K\alpha$ radiation and were subsequently discarded if any signs of crystallinity were observed.

For more detailed X-ray studies a flat mosaic of samples several foils thick was built up on a pyrex slide using thinned Duco cement. The mosaic was made thick enough to prevent penetration by the X-rays to effectively eliminate any scattering from the substrate, that is, thickness >> (mass absorption coefficient x density)$^{-1}$, so the samples could be said to be infinitely thick to the X-rays.

Accurate X-ray diffraction measurements were performed on the mosaics with a GE XRD-5 scanning diffractometer with 1.0° beam slit, 0.30° receiving slit and a 6.0° take off angle from a 1.5 mm X-ray tube spot width. An outline of the experimental arrangement is shown in figure (9).

A molybdenum $K\alpha$ (λ = 0.7107Å) X-ray source was used with a 0.04 inch thick zirconium filter which reduced the ratio of Mo $K\beta$ to Mo $K\alpha$ intensity to 0.01. A Phillips high voltage, current regulating power supply was

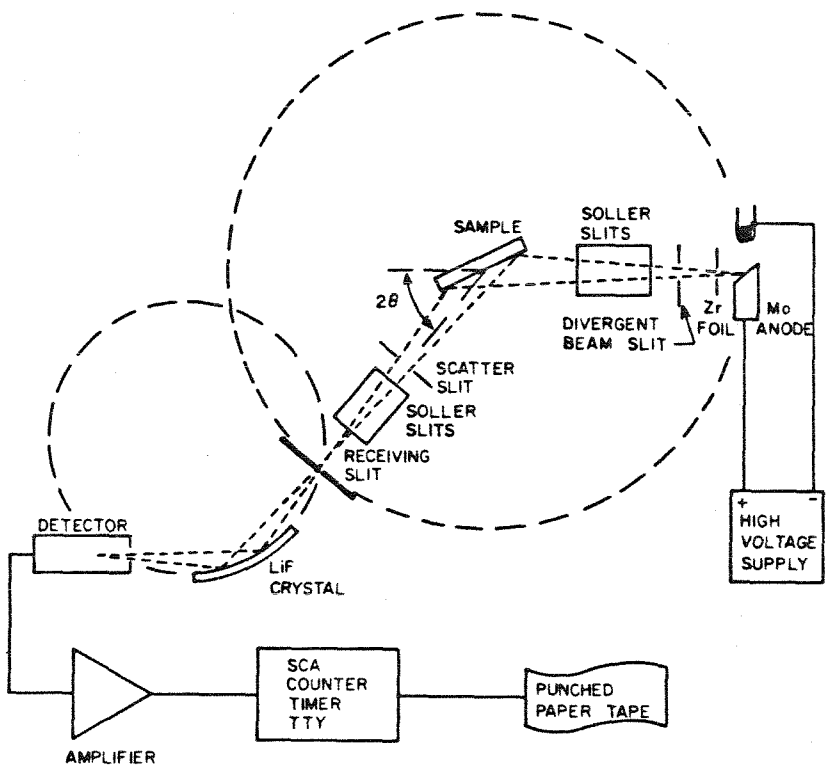

Figure 9. Experimental arrangement for X-ray diffraction measurements of flat samples.

used in a constant potential mode. Power supply and electronics stability were tested by counting for regular intervals near the Bragg peak of a crystal. The number of counts received per time interval was about 10^6 and fluctuations in output intensity were found to be less than 1% over a period of several days.

The background level of counts was measured by inserting a beam trap over the source and counting for some requisite length of time. The background was typically less than 1.5% of the total scattered counts. Air scattering contributions at angles between 6.0° and 24° were eliminated by using a specially built sample holder with mylar windows which could be evacuated by means of a mechanical pump. It was also found that placing a 3° scatter slit between the Soller slits and the sample eliminates nearly 100 percent of the air scattering without sacrificing intensity scattered from the sample. Since the diffractometer uses a Bragg-Brentano parafocussing geometry the absorption correction for an infinitely thick sample is a simple constant independent of the angle 2θ. [11]

A LiF focussing crystal monochromator is placed in the diffracted beam to eliminate scattering contributions from energies other than Mo Kα and to help reduce contributions from fluorescence and Compton scattering. The band pass function of the monochromator was measured after initial tuning to the Mo Kα characteristic line by replacing the molybdenum X-ray tube with a silver tube and scanning in energy through the Bremsstrahlung white radiation with an oriented $(10\bar{1}1)$ single crystal of quartz. Figure (10) is the band pass function which was measured in this way. With the slits described previously, the resolution of the monochromater is about 800 eV or since $E_{MoK\alpha}$ = 17.5 KeV,

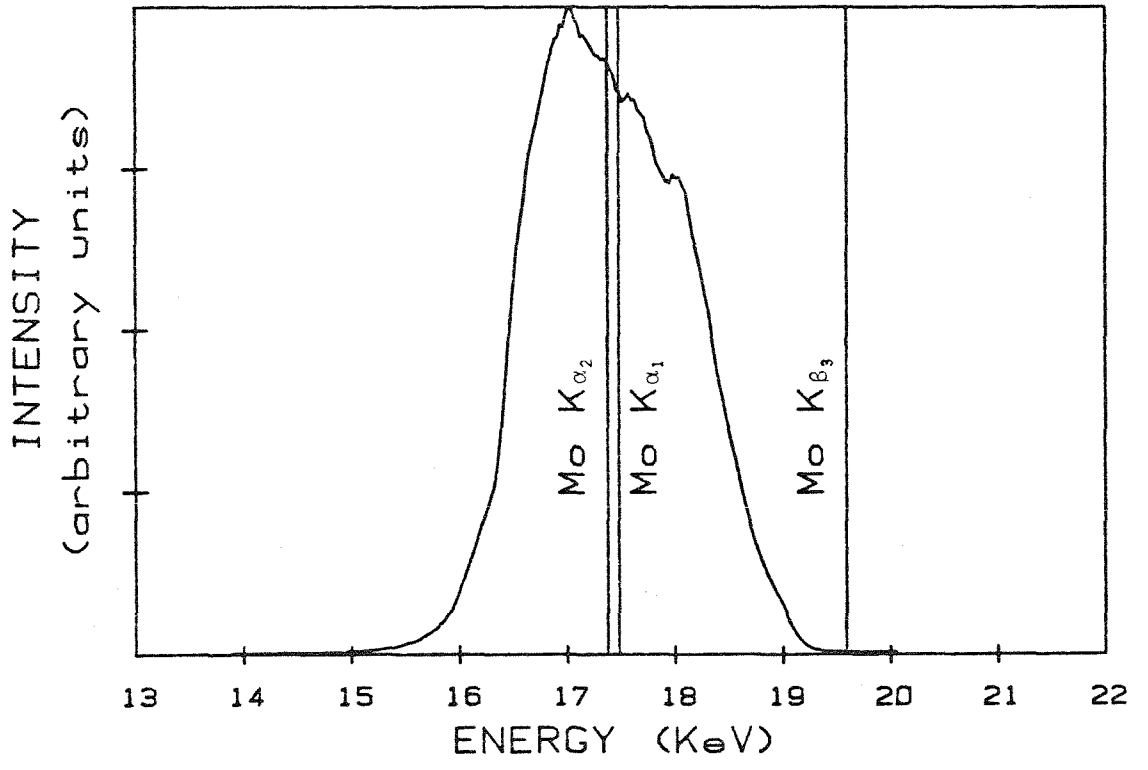

Figure 10. Experimentally measured band pass function of the focussing LiF monochromator tuned to Mo Kα radiation. Vertical lines represent the various characteristic X-ray lines of interest.

$\Delta E/E = 0.046$. Since a crystal monochromater will pass not only λ_o but also $\lambda_o/2$, $\lambda_o/3$ etc.,a NaI (Th) scintillation detector with associated electronics was used with a pulse height analyzing single channel analyzer to discriminate against all energies but the fundamental.

The X-ray diffraction profile was measured for each amorphous alloy listed in Table I. Scans were taken by counting for equal time intervals, in 2θ steps of typically 0.10° to 0.30° from 6.0° to about 80° and in 2θ steps twice as large from 80° to 160°. Digital intensity measurements for each interval were recorded automatically on punched paper tape and subsequent data reduction was performed on an IBM 370/3032 computer. The time intervals used per angle increment were typically fifteen to thirty minutes so a single scan required about one week. As many as four complete scans were taken on each sample and then added together in order to collect at least 10^4 counts per point to reduce the statistical error to less than one percent.

Densities of the amorphous metal alloys studied were measured by the hydrostatic weighing technique [51] using toluene as the working fluid. An average of the densities measured for each of three or four foils was taken for each composition.

III. RESULTS AND ANALYSIS

A. Refractory Transition Metal-Based Metallic Glasses

1) X-ray diffraction

Accurate X-ray diffraction measurements from 2θ equals 12° to 160° were made on four refractory TM-M metallic glasses of the form $(W_{0.5}Ru_{0.5})_{80}M_{20}$ where M is one of the metalloid combinations B, $B_{0.5}Al_{0.5}$, $B_{0.5}Si_{0.5}$, P. The experimentally observed diffraction intensity pattern, I_{obs}, obtained for one of these alloys, $(W_{0.5}R_{0.5})_{80}B_{20}$, is shown in figure (11) and can be expressed as

$$I_{obs}(2\theta) = I_B(2\theta) + (1/A)\cdot[I_N(2\theta) + I_c(2\theta)\cdot R(2\theta)\cdot B(2\theta)]\cdot P(2\theta).$$

In this expression I_N is the intensity of coherently scattered radiation which appeared in equation (1). I_c is the intensity of the inelastic or Compton modified radiation, which must be multiplied by the Breit-Dirac recoil function [52] $R(2\theta) = (E_{out}/E_{in})^3 = (1 + \frac{2h}{mc\lambda}\sin\theta)^{-3}$ and the experimentally measured bandpass function of the monochromator, B, which depends on the well known Compton shift in the wavelength, $\Delta\lambda = \frac{h}{mc}(1-\cos(2\theta))$. $P(2\theta)$ is the polarization factor resulting from the reflection of the X-rays from the sample through an angle 2θ and subsequently from the LiF crystal monochromator through an angle 2β. For the system used, with the monochromator in the diffracted beam, the polarization factor is given by $P(2\theta) = \frac{1}{2}(1 + \cos^2(2\beta)\cos^2(2\theta))$ and for the (200) reflection of Mo Kα radiation from LiF, 2β is about 20.3°. The background contribution I_B to the observed intensity includes electronic noise, air scattering, multiple scattering, fluorescence and stray radiation and was estimated from experimental measurements.

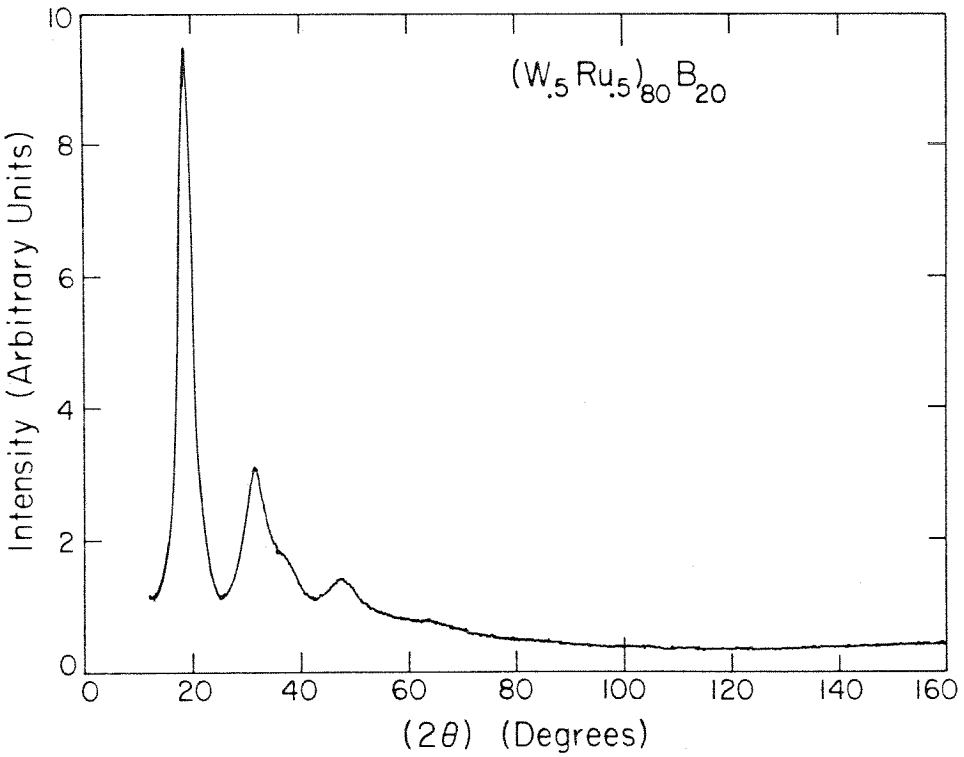

Figure 11. X-ray diffraction pattern of $(W_{0.5}Ru_{0.5})_{80}B_{20}$ metallic glass obtained using Mo Kα radiation.

Corrections for absorption were not necessary for the effectively infinite thickness samples in the geometry used.

The unknown factor A is a constant which normalizes the experimental data to electron units. To determine this normalization constant the high angle method was used. [53] It is apparent from equation (1) that for large K the total elastically scattered intensity I_N will make smaller and smaller oscillations about the average squared atomic form factor. The atomic form factors f(K) as well as their real and imaginary anomalous dispersion corrections $\Delta f'$ and $\Delta f''$ and the Compton scattering factors $I_c(K)$ have been computed by Cromer et al. [54-57] Using these tabulated values and the experimental data, the value of A was computed from a high-angle least squares fit of $I_N(K)$ to $\langle|f(K)|^2\rangle$ by requiring the minimization with respect to A of

$$\sum_{K>10}\left[A\cdot\left(\frac{I_{obs}(K)-I_B(K)}{P(K)}\right)-I_c(K)\cdot B(K)\cdot R(K)-\langle|f(K)|^2\rangle\right]^2$$

Figure (12) shows the subsequent fit of $I_N(K)$ to $\langle|f|^2\rangle$ using this method.

Once the constant A was determined the intensity function was obtained as

$$I_N(K)=A\cdot\frac{I_{obs}(K)-I_B(K)}{P(K)}-I_c(K)\cdot B(K)\cdot R(K)$$

and subsequently the interference function was found as in equation (2). I(K) for the four W-Ru alloys studied are displayed in figure (13). The curves have been smoothly extrapolated to zero for small K. The

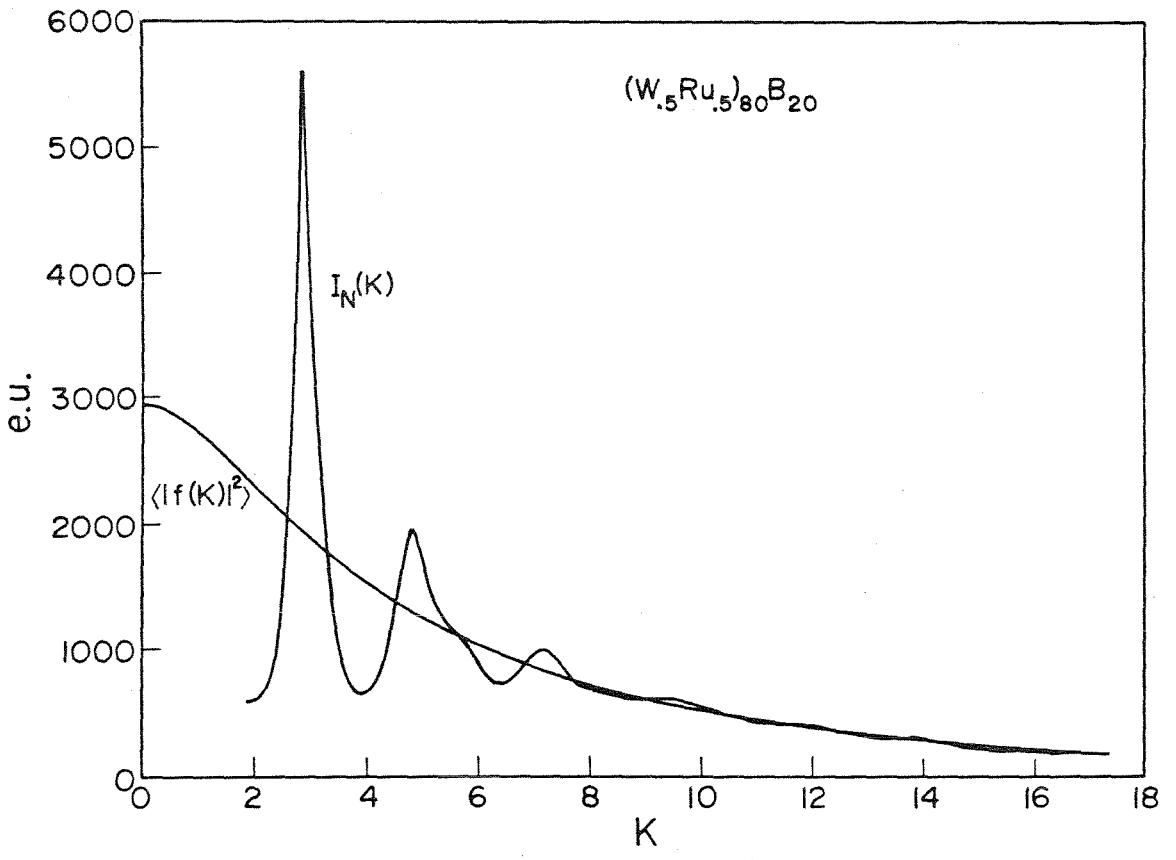

Figure 12. The total X-ray coherent scattering intensity of $(W_{0.5}Ru_{0.5})_{80}B_{20}$ metallic glass normalized to electron units/atom by fitting to $\langle|f(K)|^2\rangle$ above K = 10 $\AA^{-1}$ [A. Williams and W. L. Johnson, J. Non-Cryst. Solids 34, 121 (1979)].

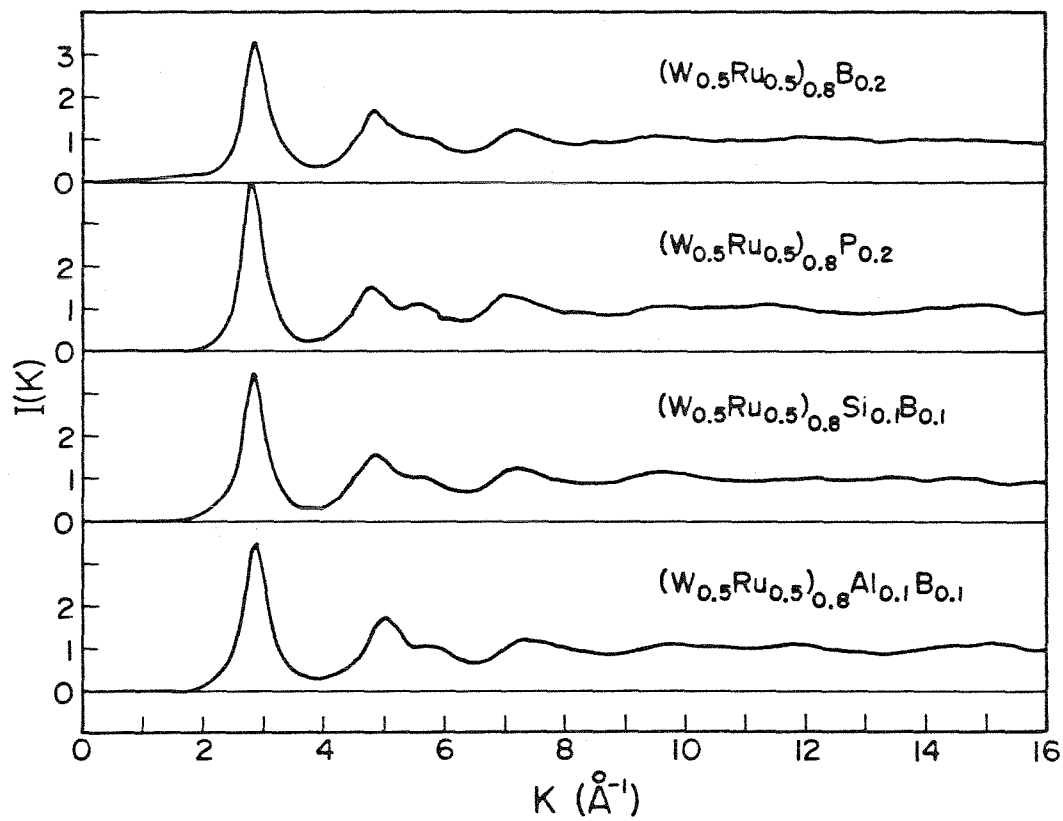

Figure 13. X-ray interference functions I(K) of four W-Ru based metallic glasses.

general shape of the curves is very similar for all four alloys, the single large primary maximum and shoulder on the high-K side of the smaller second band being in particular very common to the I(K) of amorphous TM-M alloys. The features die out quite rapidly with increasing K, and from the width of the primary diffraction band (~0.5 $\mathring{A}^{-1}$ FWHM) the Scherrer formula [11] reveals an average scattering particle size of about 13 Angstroms, typical of amorphous metals. Lack of significant short range order beyond about 13 $\mathring{A}$ is often taken as the definition of an amorphous metal structure, while metals with ordering extending to 50 or 100 $\mathring{A}$ are generally considered micro-crystalline.

The quantity K(I(K)-1), which is the interesting function for the sine transform of equation (3), is often called the reduced interference function i(K). In reality the integral from zero to infinity in equation (3) must be terminated at a finite value of K, which for these experiments, (with Mo Kα radiation), is about 17.4 $\mathring{A}^{-1}$. Such an abrupt termination of the transform however, when i(K) has not yet converged, produces false termination satellites in G(r). A less abrupt window in the form of an exponential convergence factor of the form e^{-bK^2} is therefore often used for the transform to reduce the magnitude of these termination ripples at the expense of broadening the G(r). In effect, if we can write

$$G(r) = \frac{2}{\pi}\int_0^{\infty} K(I(K)-1)\sin(Kr)dK$$

and

$$G'(r) = \frac{2}{\pi}\int_0^{K_{max}} K(I(K)-1)e^{-bK^2}\sin(Kr)dK$$

then the function G'(r) becomes a convolution of the true transform G(r) with some modifying function $Q(r,\gamma)$

$$G'(r) = \frac{K_{max}}{\pi}\int_0^{\infty} Q(r'-r,\gamma)G(r')dr'$$

where $\gamma^2 = bK^2_{max}$. Warren [11] has given approximate solutions for the modifying function $Q(r,\gamma)$ and some of these curves are plotted in figure (14) for various values of b using $K_{max} = 17.4$ Å^{-1}. The suppression of the termination ripples in G(r) as well as the associated broadening of its features are illustrated in figure (15) for $(W_{0.5}Ru_{0.5})_{80}B_{20}$ using several different values of b. Figures (16) and (17) show the i(K) and G(r) obtained for each of the four W-Ru based metallic glasses studied here. "Fuzziness" in the high K region of the i(K) due to instrumental and statistical fluctuations in the data was eliminated through the use of a smoothing algorithm. The G(r) shown were computed using a convergence factor of b = 0.005 which involves a broadening of about 0.28 Å FWHM. The single large maximum and double peaked second band which are obvious in each case are very common features of the G(r) for amorphous TM-M alloys.

The differences existing between the reduced radial distribution functions of the four refractory transition metal based glassy alloys are presumably the result of structural differences in the transition metal matrix, since metalloid contributions to the scattering are quite small. W-Ru-B and W-Ru-P appear to be very similar, while W-Ru-Si-B exhibits considerably blunted and widened second and third maxima. W-Ru-Al-B is particularly aberrant in that the third peak is actually

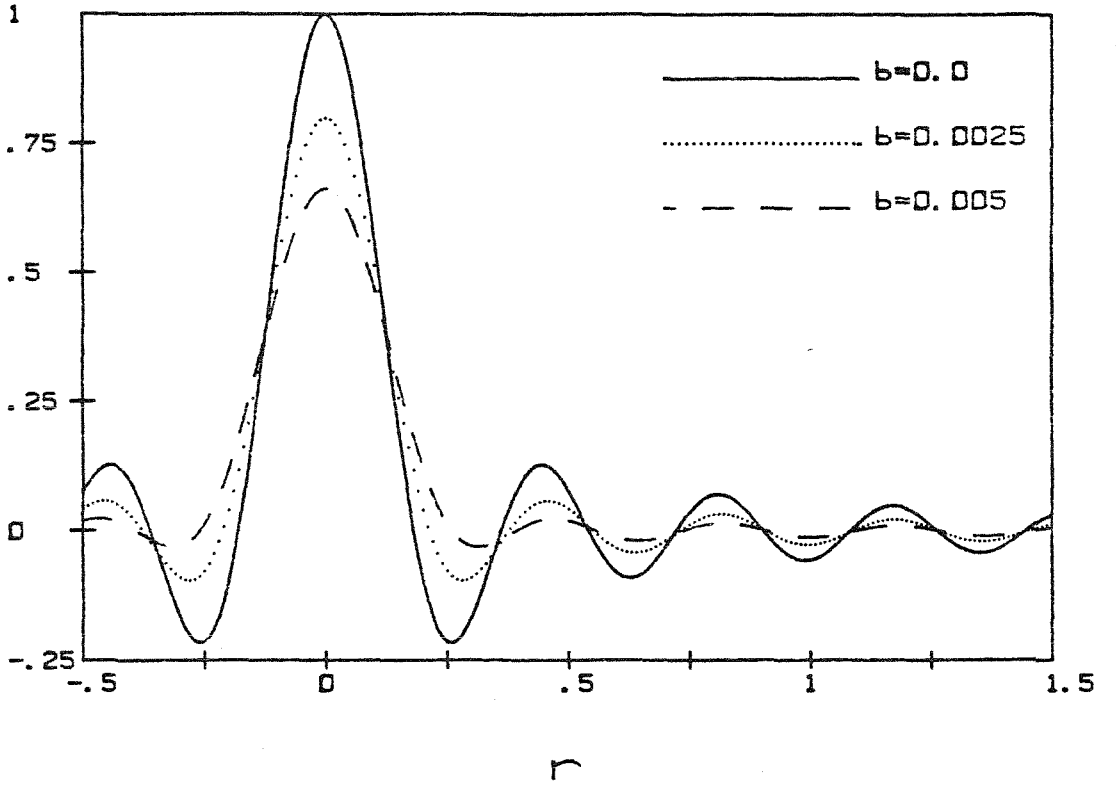

Figure 14. Modifying function $Q(r,\gamma)$ which represents combined effects of termination at K_{max} and exponential damping with convergence factor $\exp(-bK^2)$ of Fourier transform on the resulting reduced radial distribution function $G(r)$. The value of K_{max} is 17.4 $\mathring{A}^{-1}$ and $\gamma^2 = bK_{max}^2$.

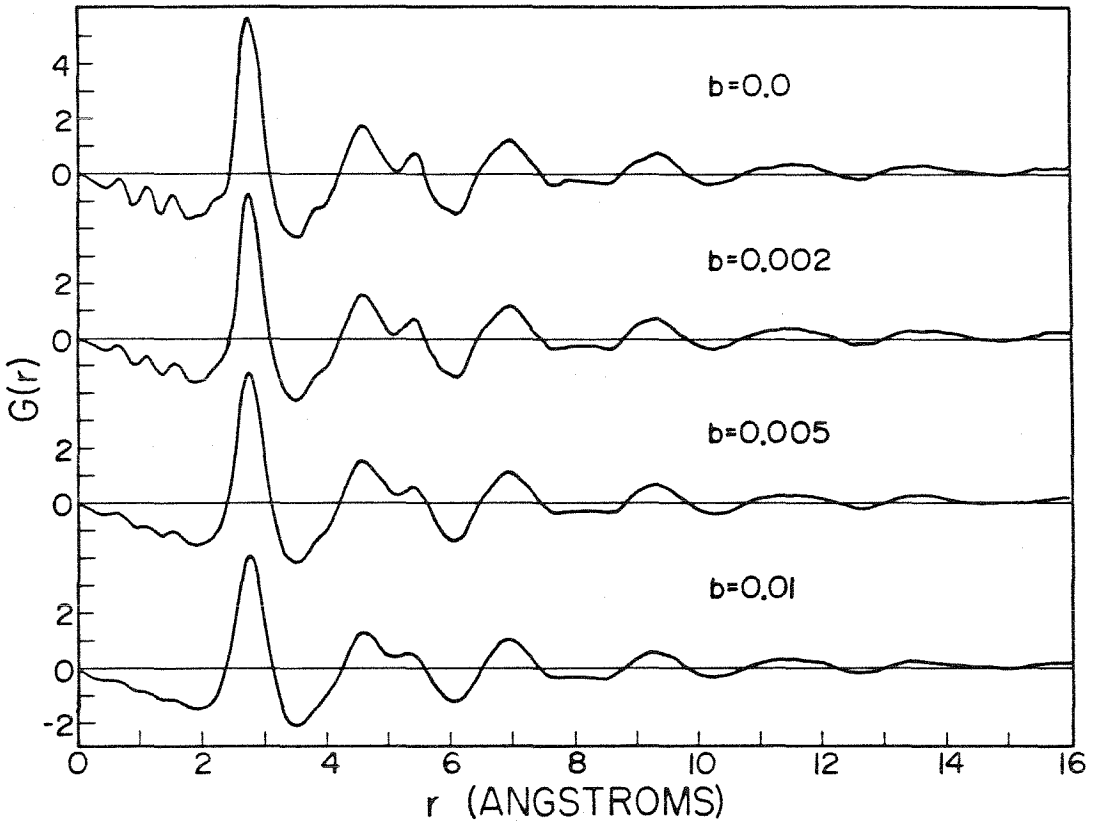

Figure 15. Effect on reduced radial distribution function G(r) of $(W_{0.5}Ru_{0.5})_{80}B_{20}$ metallic glass of applying an exponential convergence factor $\exp(-bK^2)$ to the Fourier transform of the reduced interference function i(K).

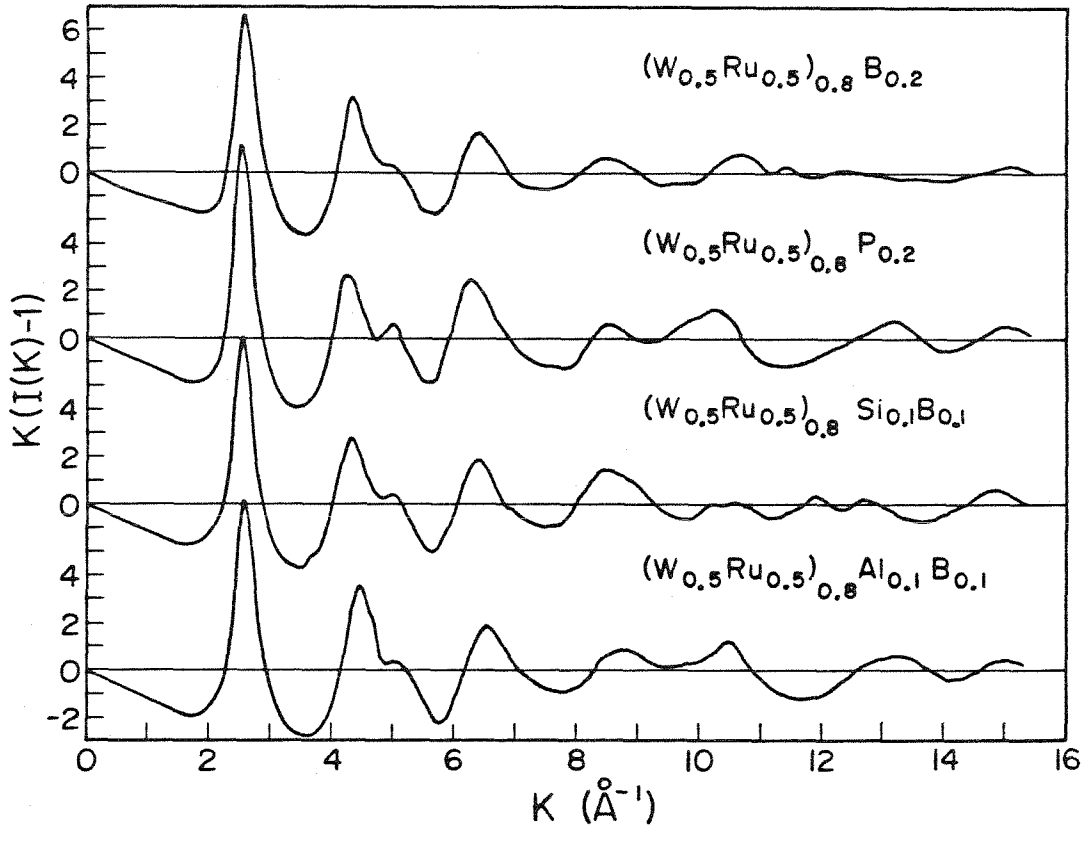

Figure 16. X-ray reduced interference functions i(K) = K(I(K)-1) of four W-Ru based metallic glasses.

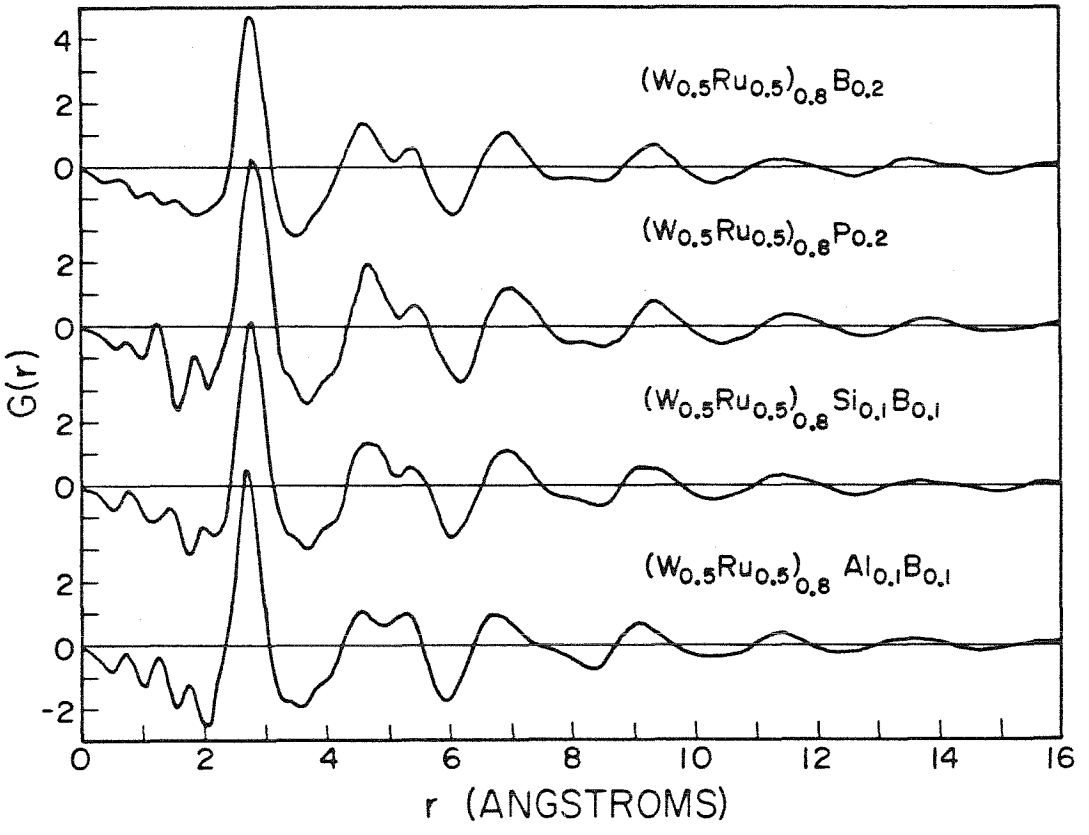

Figure 17. Reduced radial distribution functions $G(r) = 4\pi r\,[\rho(r)-\rho_0]$ of four W-Ru based metallic glasses obtained from X-ray data and using a convergence factor $\exp(-0.005\ K^2)$ [A. Williams and W. L. Johnson, J. Non-Cryst. Solids 34, 121 (1979)].

slightly larger than the second, an unusual situation for amorphous TM-M alloys. Also the G(r) appears to be slightly contracted for W-Ru-Al-B, the peaks occurring at slightly smaller values of r (about 2%), than for the other alloys. Since aluminum has a considerable solid solubility in W and Ru (about 15 atomic percent, compared to <0.1% for boron) it is possible that it can enter substitutionally in the metallic glass which has been rapidly quenched from the melt. Substitution would be very unlikely for the smaller, less soluble metalloids such as phosphorous and boron. From figure (17) then, the structure of the TM-M metallic glass appears to be strongly dependent on the size and electronegativity of the metalloid constituents.

The positions of the first four maxima in the $\rho(r)$ are listed in table (II) along with widths of the primary bands corrected for broadening from $Q(r,\gamma)$. The values shown for R_2/R_1 and R_3/R_1 are very typical for amorphous TM-M alloys. Also included are first nearest neighbor coordination numbers computed as

$$n = \int_0^{R_0} 4\pi r^2 \rho(r) dr$$

where R_0 is the minimum following the primary maximum of $\rho(r)$. The function $4\pi r^2\rho(r)$ in the integrand above is called the radial distribution function, or RDF.

The position of the primary maximum in the density function corresponds to the nearest neighbor distance. Except for W-Ru-Al-B this distance is slightly larger than twice the average Goldschmidt radius of W and Ru, (2.75 Å). The second maxima occur at a distance

Alloy	R_1(Å) ±0.02	ΔR_1(Å) (FWHM) ±0.02	R_2/R_1 ±0.02	R_3/R_1 ±0.02	R_4/R_1 ±0.03	η ±0.45	ρ_0 (atoms/Å^3) ±0.0007
$(W_{0.5}Ru_{0.5})_{0.8}B_{0.2}$	2.76	0.21	1.66	1.96	2.52	11.58	0.07598
$(W_{0.5}Ru_{0.5})_{0.8}Al_{0.1}B_{0.1}$	2.72	0.19	1.68	1.95	2.48	11.92	0.07541
$(W_{0.5}Ru_{0.5})_{0.8}Si_{0.1}B_{0.1}$	2.77	0.20	1.69	1.94	2.50	11.76	0.07081
$(W_{0.5}Ru_{0.5})_{0.8}P_{0.2}$	2.80	0.22	1.68	1.96	2.51	12.59	0.07174
DRPHS	2.75	-	1.73	1.99	2.65	12	0.05783

Table II. Atomic densities, peak positions and widths of primary peak of $\rho(r)$, and average first nearest neighbor coordination number of W-Ru based metallic glasses and Finney's DRPHS. [27]

about 1.68 times the nearest neighbor distance, and if contributions from the overlapping third peak of G(r) are subtracted by fitting the doubly peaked second band to a pair of Gaussians, the values of R_2/R_1 in table (II) for the W-Ru alloys decrease by about 0.025. The R_2/R_1 are therefore close to the separation 1.633, occurring between opposite apices of two tetrahedra sharing a common base (figure (8)). This configuration occurs on the pentagonal rings of an icosohedron as illustrated in figure (18), but not in a DRPHS. The third peak position occurs at slightly less than twice the nearest neighbor distance for the metallic glasses. Three nearly collinear transition metal atoms are the responsible configuration, which also occurs in the icosohedron.

The DRPHS G(r) produced by Finney [27] in the form of a histogram is plotted on top of the G(r) obtained for $(W_{0.5}Ru_{0.5})_{80}B_{20}$ in figure (19) using a hard sphere diameter, d, of 2.75 Å as the only adjustable parameter. The model is a reasonably good qualitative fit to the experimentally obtained data, which are essentially (96%) a distribution function of the transition metal atoms only. Quantitatively, however, the agreement is not quite as impressive and data from the DRPHS are included in table (II). The relative peak heights of the third and second maxima are reversed in the DRPHS; however this discrepancy has been found by most computer and laboratory modelers to be relatively easy to correct by relaxing the dense random packing. The relative peak positions of the second and third maxima are larger in the model than for the metallic glass and correspond to the commonly occurring configurations in Bernal's pseudonuclei. [26] $R_2/R_1 = 1.73$ is the separation of opposite vertices of two tetrahedra with coplanar bases

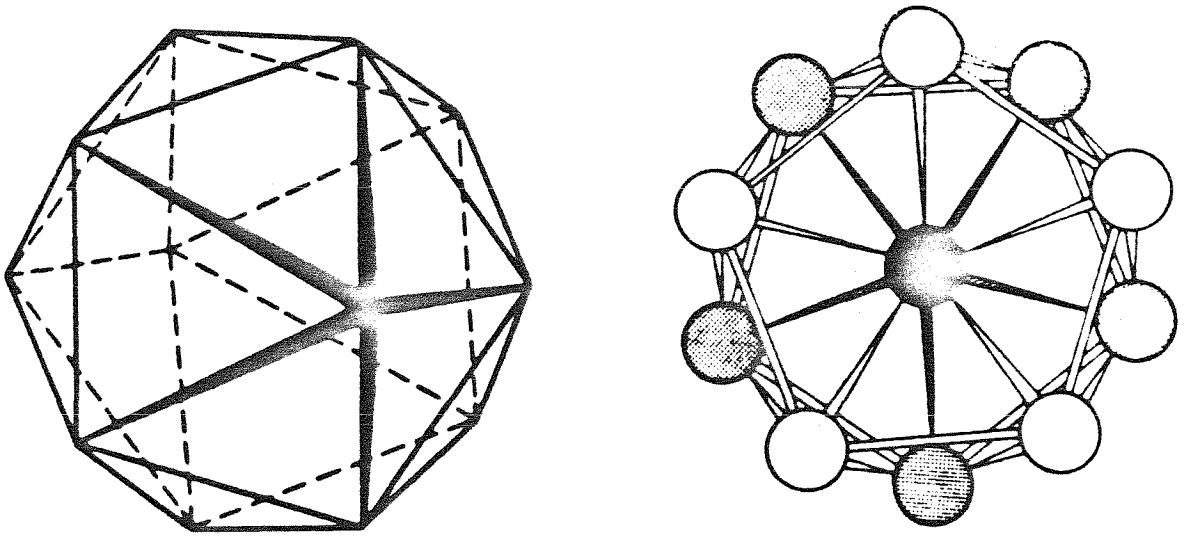

Figure 18. Icosohedron (a) and its projection (b) normal to the five-fold axis, from A. K. Sinha [Prog. Mat. Sci. 15, 79 (1972)].

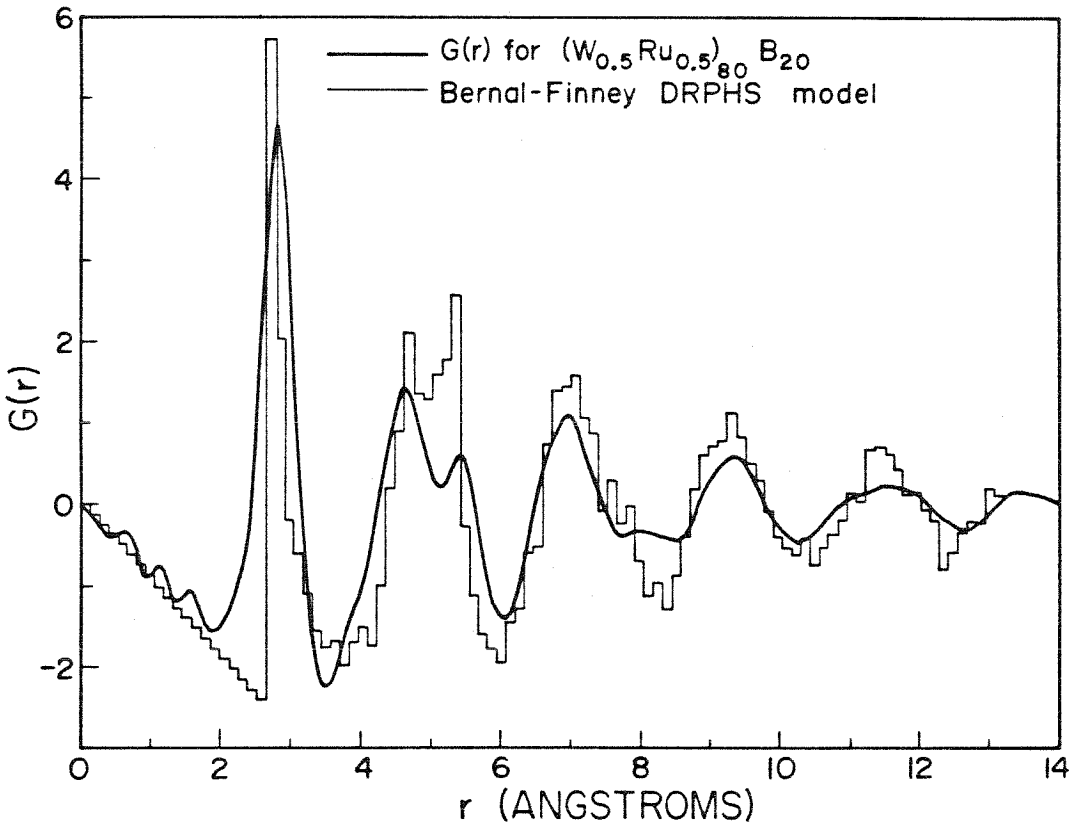

Figure 19. A comparison of the reduced radial distribution function of $(W_{0.5}Ru_{0.5})_{80}B_{20}$ metallic glass and of the Finney DRPHS [A. Williams and W. L. Johnson, J. Non-Cryst. Solids 34, 121 (1979)].

(figure (8)) and is a configuration which does not occur in an icoschedral cluster. The position of the third peak is very nearly equal to twice the nearest neighbor distance, the hard sphere collineations in the Bernal-Finney model being very nearly perfect a large percentage of the time.[26] Binary dense random packings of spheres of two different sizes and relaxed hard sphere models have had little success in reducing the values of R_2/R_1 and R_3/R_1 to values more in agreement with observation, [31-33] and hard sphere models which try to incorporate an icosohedral cluster type structure have been found to be impossible to pack into a dense configuration. Bernal has shown that a packing of icosohedral clusters (spherically polytetrahedral arrangement) is inconsistent with a dense random packing of hard spheres [26], in which insufficient volume is available to allow the formation of many distorted icosohedra and their associated inter-cluster voids. Computer generated, relaxed models with softer potentials (Lennard-Jones, Morse) have had the most success [33] in reproducing R_2/R_1 and R_3/R_1 but still fall short by 5 to 10% of achieving the high atomic densities observed for metallic glasses.

Using the approximation introduced in equation (3) allows the G(r) to be expressed as a linear combination of the pair density functions, $\rho_{ij}(r)$. Treating the alloys as quasi-binary systems with constituents labeled TM or M allows the total G(r) to be written in each case as

$$G(r) = 4\pi r\,[\rho(r)-\rho_0]$$

with

B	$\rho(r) = 1.199\rho_{TM-TM}(r) + 0.406\rho_{TM-M}(r) + 0.002\rho_{M-M}(r)$
B-Al	$\rho(r) = 1.160\rho_{TM-TM}(r) + 0.708\rho_{TM-M}(r) + 0.007\rho_{M-M}(r)$
B-Si	$\rho(r) = 1.155\rho_{TM-TM}(r) + 0.744\rho_{TM-M}(r) + 0.008\rho_{M-M}(r)$
P	$\rho(r) = 1.105\rho_{TM-TM}(r) + 1.124\rho_{TM-M}(r) + 0.018\rho_{M-M}(r)$

The coordination numbers obtained from the RDF's of the metallic glasses are linear combinations of the individual pair coordination numbers with coefficients given as above. A first order approximation for n_{TM-TM} is to divide the computed n by the coefficient of $\rho_{TM-TM}(r)$ in the above equations, ignoring the contributions from n_{TM-M} and n_{M-M}. This approximation is best for the W-Ru-B alloy, which has the smallest coefficients for the metalloid components of n and for which it yields $n_{TM-TM} = 9.66$. This is quite short of the 12-fold coordinated DRPHS and cannot be explained if metalloids are assumed purely interstitial. In the next order of approximation the contributions of n_{MM} alone are neglected (a good approximation) and the assumption is further made that the W-Ru-B, W-Ru-B-Si, and W-Ru-P metallic glasses are isostructural on the basis of the similarity in their reduced radial distribution functions. W-Ru-Al-B is excluded due to the several anomalous characteristics of its G(r), including the smallness of R_1, the kink on the small r side of the primary maximum and the peculiar second band, (for which W-Ru-Si-B is, as well, probably only marginal at best). Writing

$$n_B = 11.58 = 1.199n_{TM-TM} + 0.406n_{TM-M}$$

$$n_{B-Si} = 11.76 = 1.155n_{TM-TM} + 0.744n_{TM-M}$$

$$n_P = 12.59 = 1.105n_{TM-TM} + 1.124n_{TM-M}$$

the three solutions for n_{TM-TM} and n_{TM-M} that can be obtained assuming alloy isomorphism are shown in table (III) with results obtained by Sadoc and Dixmier [42] for electrodeposited $Co_{81}P_{19}$ using combined neutron and X-ray diffraction data. The values obtained from the W-Ru data have large fluctuations but are reasonably consistent in view of the many approximations made, in particular the isomorphism of the alloys. The total transition metal coordination, n_{TM} is always close to 11 for the W-Ru glasses, which is under-coordinated for an icosohedron and it seems more likely that n_{TM-TM} is closer to the value 9.66 which was estimated from W-Ru-B alone. Both the Co-P and W-Ru alloys show about two metalloid near neighbors to transition metals.

2) Density measurements of Mo-Ru based metallic glasses

The similarity of the phase diagrams and lattice parameters of the intermetallic compounds (tetragonal σ phase) [58-59] of the W-Ru and Mo-Ru systems, as well as very close agreement in the atomic densities of their glassy alloys,[49] suggests that a detailed study of the environments of Mo (W) and Ru in their metallic glasses might be made by utilizing X-ray diffraction data from various alloys in which Mo and W are substituted for each other. This type of experiment was attempted but found to be impractical with the available experimental facilities due to severe signal to noise degradation from Mo fluorescence when using a Mo X-ray tube and from Ru fluorescence when using a Ag X-ray tube. Density measurements were found to be enlightening however on $(Mo_{0.6}Ru_{0.4})_{1-x}M_x$ alloys which have a considerably lower melting point than the W-Ru alloys and are known to be quenchable into a glassy state over a wide range of x with both M = B and M = Si. [49]

Alloy Pair	n_{TM-TM}	n_{TM-M}	$n_{TM} = n_{TM-TM} + n_{TM-M}$	n_{M-TM}
$B\text{-}B_{0.5}Si_{0.5}$	9.16	1.46	10.62	5.84
B - P	8.79	2.56	11.35	10.23
$B_{0.5}Si_{0.5}$ - P	8.05	3.29	11.34	13.16
average	8.67 $\pm$ 0.57	2.44 $\pm$ 0.92	11.10 $\pm$ 0.42	9.74 $\pm$ 3.68
$Co_{81}P_{19}$	10.1	2.09	12.2	8.9
Polk	12	-	-	-

Table III. Partial pair nearest neighbor coordination numbers obtained by Sadoc and Dixmier [42] for amorphous electrodeposited $Co_{81}P_{19}$ and those obtained by assuming isomorphism for pairs of $(W_{0.5}Ru_{0.5})_{80}M_{20}$ metallic glasses where M = B, $B_{0.5}Si_{0.5}$, P.

Densities have been measured on a number of these metallic glasses [49] which were prepared in the manner previously described. The results in table (IV) demonstrate a steady increase in atomic density with increasing metalloid concentration x. This is in line with the Polk picture of metalloid atoms filling up Bernal holes in a distorted dense random packing. In this picture the DRP matrix of transition metal atoms would be expected to have a constant or slowly varying density ρ_{TM} equal to $(1-x)\rho_0$, which is included in table (IV) and is relatively slowly varying for Mo-Ru-B for which it decreases by only about 5% throughout the composition range of formability of the metallic glass, while the bulk atomic density increases by more than 13% over the same range. Mo-Ru-Si on the other hand exhibits an 11% decrease in ρ_{TM} and only a 5% increase in ρ. This strongly suggests that something more subtle than hole filling is occurring, which is dependent on the type of metalloid.

Figures (20) and (21) are plots of the average atomic volume $\overline{V}$ versus x for $(Mo_{0.6}Ru_{0.4})_{1-x}B_x$ and $(Mo_{0.6}Ru_{0.4})_{1-x}Si_x$ respectively. The data are approximately linear and were least squares fitted into a line $\overline{V} = b + mx$ with constants given as

$$\overline{V} = 15.34 - 11.40\ x\ (\mathring{A}^3) \quad (Mo_{0.6}Ru_{0.4})_{1-x}B_x$$

$$\overline{V} = 15.32 - 4.36\ x\ (\mathring{A}^3) \quad (Mo_{0.6}Ru_{0.4})_{1-x}Si_x$$

If we assume constant atomic volumes V_{TM} and V_M for transition metal and metalloid atoms respectively then

$$\overline{V} = (1-x)V_{TM} + (x)V_M \qquad \text{so} \qquad V_{TM} = b \text{ and } V_M = m + b.$$

Alloy	ρ gm/cm^3 ($\pm$0.05)	ρ atoms/Å^3 ($\pm$.0007)	$\rho\cdot(1-x)$ atoms/Å^3 ($\pm$.001)	$\overline{V}$ Å^3 ($\pm$.15)
$(M_{0.6}Ru_{.4})_{1-x}B_x$				
x = 0.10	10.49	0.07072	0.06365	14.14
0.12	10.48	0.07210	0.06345	13.87
0.14	10.28	0.07215	0.06205	13.86
0.16	10.33	0.07396	0.06213	13.52
0.18	10.19	0.07452	0.06110	13.42
0.20	10.15	0.07587	0.06070	13.18
0.22	10.33	0.07886	0.06151	12.68
0.24	10.14	0.07918	0.06017	12.63
$(M_{0.6}Ru_{.4})_{1-x}Si_x$				
x = 0.18	9.79	0.06897	0.05655	14.50
0.20	9.67	0.06930	0.05541	14.43
0.22	9.56	0.06969	0.05436	14.35
0.24	9.45	0.07008	0.05326	14.27
0.26	9.26	0.06988	0.05171	14.31
0.28	9.15	0.07027	0.05060	14.23
0.30	9.19	0.07184	0.05029	13.92
0.32	9.07	0.07220	0.05054	13.85

Table IV. Mass densities, atomic densities and mean atomic volumes of $(Mo_{0.6}Ru_{0.4})_{1-x}B_x$ and $(Mo_{0.6}Ru_{0.6})_{1-x}Si_x$ metallic glasses. (49)

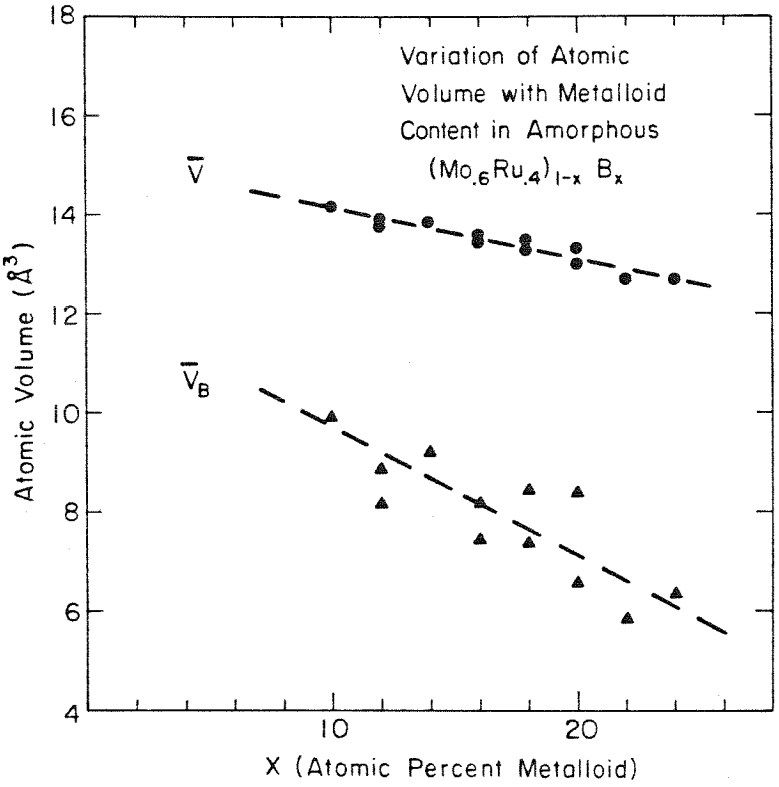

Figure 20. Variation of mean atomic volume $\overline{V}$ and effective boron volume $\overline{V}_B$ with boron concentration for $(Mo_{0.6}Ru_{0.4})_{1-x}B_x$ metallic glasses [W. L. Johnson and A. Williams, Phys. Rev. B 20, 1640 (1979)]. $\overline{V}_B$ calculated as prescribed by D. Turnbull [Scr. Metall. 11, 1131 (1977)].

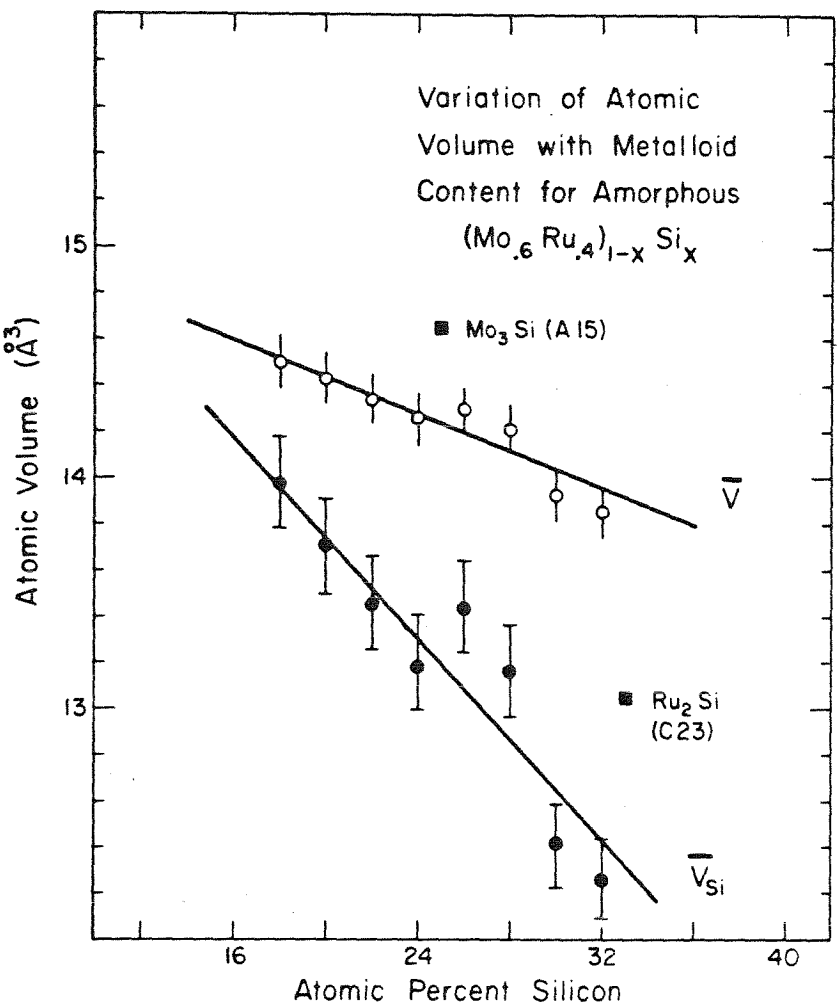

Figure 21. Variation of mean atomic volume $\bar{V}$ and effective silicon volume $\bar{V}_{Si}$ with silicon concentration for $(Mo_{0.6}Ru_{0.4})_{1-x}Si_x$ metallic glasses [W. L. Johnson and A. Williams, Phys. Rev. B 20, 1640 (1979)]. $\bar{V}_{Si}$ calculated as prescribed by D. Turnbull [Scr. Metall. 11, 1131 (1977)].

Then

V_{TM}	V_M	
15.34 $\mathring{A}^3$	3.94 $\mathring{A}^3$	for Mo-Ru-B
15.32 $\mathring{A}^3$	10.96 $\mathring{A}^3$	for Mo-Ru-Si

The excellent agreement between the values of V_{TM} invites the suggestion that this is the average atomic volume of a pure $Mo_{0.6}Ru_{0.4}$ amorphous matrix. Using the average from the two alloy systems above gives V_{TM} = 15.33 $\mathring{A}^3$ and an atomic density of 0.06523 atoms/$\mathring{A}^3$. Using the average Goldschmidt radius of 1.37 Angstroms this is a packing efficiency $\eta = \frac{4}{3}\pi r_G^3/\overline{V}_{TM}$ = 0.7026 for the "pure" $Mo_{0.6}Ru_{0.4}$ amorphous matrix. Further, data collected from a number of studies of amorphous TM-M alloys where density measurements were reported suggest that this value is universal to these systems. Table (V) displays V_{TM}, V_M, and the packing fraction, η, which were calculated from data for nine systems of amorphous TM-M alloys. The packing fractions obtained from the extrapolations are very nearly the same in every case, the average value being 0.7001 with a standard deviation of only about 1%. This value may be considered then to be the packing efficiency of the ideal, pure amorphous transition metal, and is still considerably larger (9%), than that obtained from the DRPHS models.

The atomic volume of boron in $(Mo_{0.6}Ru_{0.4})_{1-x}B_x$ is given as 3.94 $\mathring{A}^3$. If the transition metal packing efficiency is used to estimate the metalloid size then $\frac{4}{3}\pi r_G^3$ = (.70) (3.94 $\mathring{A}$) yields r_B = 0.87 $\mathring{A}$, a value between the atomic and covalent radius of boron, (0.98 and 0.82 $\mathring{A}$ respectively). For the case of $Fe_{1-x}B_x$ (from table (V)) the value

Alloy System	V_{TM}	V_M	n	Reference
$Fe_{1-x}B_x$	11.84	5.15	0.7074	a)
$Fe_{1-x}P_x$	12.02	11.61	0.6973	b)
$Ni_{1-x}P_x$	11.12	11.01	0.7183	c)
$Co_{1-x}P_x$	11.86	8.29	0.6898	d)
$La_{1-x}Ga_x$	39.20	10.50	0.6988	e), f)
$La_{1-x}Al_x$	39.69	11.94	0.6901	g)
$(Pd_{0.6}Cu_{0.4})_{1-x}P_x$	14.33	11.76	0.6939	f)
$(Mo_{0.6}Ru_{0.4})_{1-x}B_x$	15.34	3.94	0.7021	f)
$(Mo_{0.6}Ru_{0.4})_{1-x}Si_x$	15.32	10.96	0.7031	f)
Average	-	-	0.7001 $\pm$ 0.009	

a) R. Ray, R. Hasegawa, C. P. Chou, and L. A. Davis, Scr . Metall. 11, 973 (1977).

b) J. Logan, Phys. Stat. Sol. (a) 32, 361 (1975).

c) G. S. Cargill III, J. Appl. Phys. 41, 12 (1970).

d) G. S. Cargill III and R. W. Cochrane, J. de Physique 35, C4-269 (1974).

e) W. H. Shull, D. G. Naugle, S. J. Poon and W. L. Johnson, Phys. Rev. B 18, 3263 (1978).

f) W. L. Johnson and A. Williams, Phys. Rev. B 20, 1640 (1979).

g) A. Williams, unpublished results.

Table V. Results of straight line, $\overline{V} = (1-x)\overline{V}_{TM} + \overline{V}_M$, least squares fit to the mean atomic volumes, $\overline{V}$, of some amorphous transition metal-metalloid alloys as a function of metalloid concentration, and the resulting packing fraction, n, at x = 0.

obtained is r_B = 0.95 Å, also between the covalent and atomic radii of B. For the alloys Fe-P, Ni-P, Co-P, and Pd-Cu-P the values for r_P are 1.25 Å, 1.23 Å, 1.11 Å, and 1.25 Å respectively, again always between the atomic, (1.28 Å), and covalent (1.06 Å) radii of the metalloid. Clearly then, there appears to be some covalency and charge transfer involved in the transition metal-metalloid bonds in these amorphous alloys.

The pair density functions for the refractory transition metal-metalloid glasses investigated here demonstrate the occurrence of the atomic separations and coordination number which occur for distorted icosohedra. The average transition metal coordination is between 11 and 12 with about 2 of the neighbors being metalloid atoms. The metallic glass structure is apparently sensitive to metalloid type, although the role of metalloids in these systems is still largely not understood. It seems clear that the Polk model is at best a gross oversimplification of the situation and such features as size, electronegativity, valence and concentration of metalloids are important considerations to their behavior. The dense collection of distorted icosohedra comprising the metallic glasses has only a superficial resemblence to the aggregation of twisted tetrahedral spirals of the DRPHS models, and it is not likely that any model using hard sphere potentials will be able to recreate the structure of amorphous TM-M alloys. Workable models of binary amorphous alloys will have to incorporate more realistic (than hard spheres) sets of interatomic potentials, including a metalloid-metalloid interaction and a semi-covalent transition metal-metalloid interaction in order to reproduce the high density and short range topology of amorphous TM-M alloys. Matching the packing density .7001 of the proposed ideal single constituent

amorphous metal to that of a single component dense random packing can serve as a natural starting place for such modelling.

B. Lanthanum Based Metallic Glasses

Lathanum and its compounds and alloys have been the subjects of some study in the past as a result of their unusual structural and electronic properties. There are two allotropic forms of La, the double HCP (α-La) structure and the FCC (β-La) structure, the former transforming completely to FCC above 292° C or above 23 Kbar of pressure at room temperature. [59] Considering its position in the periodic table, La has an anomalously low melting point (920° C, as compared to > 1500° C for Sc, Y, and Lu) and high superconducting transition temperature (4.9° K and 6.1° K for α-La and β-La respectively). It also has a negative thermal expansion coefficient at low temperature, [60] a non-linear high temperature resistivity [61] and a relatively low electronegativity, being one of the most chemically active of the rare earth metals. Elemental lanthanum will react directly with water, oxygen, nitrogen, carbon, boron, selenium, silicon, phosphorus and the halogens. Lanthanum and several of its intermetallic compounds such as La_3Al and LaCu have extremely high positive pressure coefficients of superconducting T_c,[62] La itself, at 150 Kbar, having a T_c of 12° K,[63] the highest of any elemental superconductor.

A number of lanthanum based metallic glasses have been produced in recent years including alloys with Au, Cu, Ni, [64] Ge, Al, [65] Ag, [66] Ga, [67] and In, [68] and several studies of the electronic and superconducting properties have been reported. [64-67] Only one complete X-ray diffraction study has been performed on a glassy lanthanum alloy

however, [69] presumably due to the rapid rate of deterioration of these systems in air due to oxidation and attack by water vapor. An amorphous foil of $La_{80}Au_{20}$, for example, became tarnished after only one hour in air and crystal Bragg peaks appeared in the X-ray diffraction pattern after only 12 hours. At the end of 72 hours in air the foil was black and beginning to disintegrate and no trace of an amorphous band could be distinguished in the diffraction pattern, which consisted of sharp peaks identified as hexagonal $La(OH)_3$. It is interesting to note that no trace of a diffraction peak could be observed at that time for Au or any La-Au compound, suggesting that a Au-rich amorphous phase still remained after leaching out of a substantial fraction of the more reactive La.

In this study, accurate X-ray diffraction measurements from 2θ = 6.0 to 160 degrees were made on twelve amorphous alloys of La with Al, Ga, and Au at the compositions indicated in table (I). i(K) was computed in each case in the manner previously described. The four reduced interference functions for each of the three compositions studied are displayed in figures (22), (23), and (24), and appear to be not too unlike those of many amorphous TM-M alloys. The La-Au alloys are exceptional in that they exhibit considerably less structure than the others, and Logan [69] has suggested that the scattering contribution from La-Au pairs interferes with the La-La scattering, which is predominant in the alloys with lower-Z constituents. Also unique to La-Au is a distinct prepeak in the intensity function, $I_N(K)$, as shown in figure (25) for $La_{76}Au_{24}$. No such prepeak was reported by Logan for $La_{80}Au_{20}$, possibly because he began his scan at an insufficiently small angle. While very small prepeaks appear also for $La_{72}Ga_{28}$,

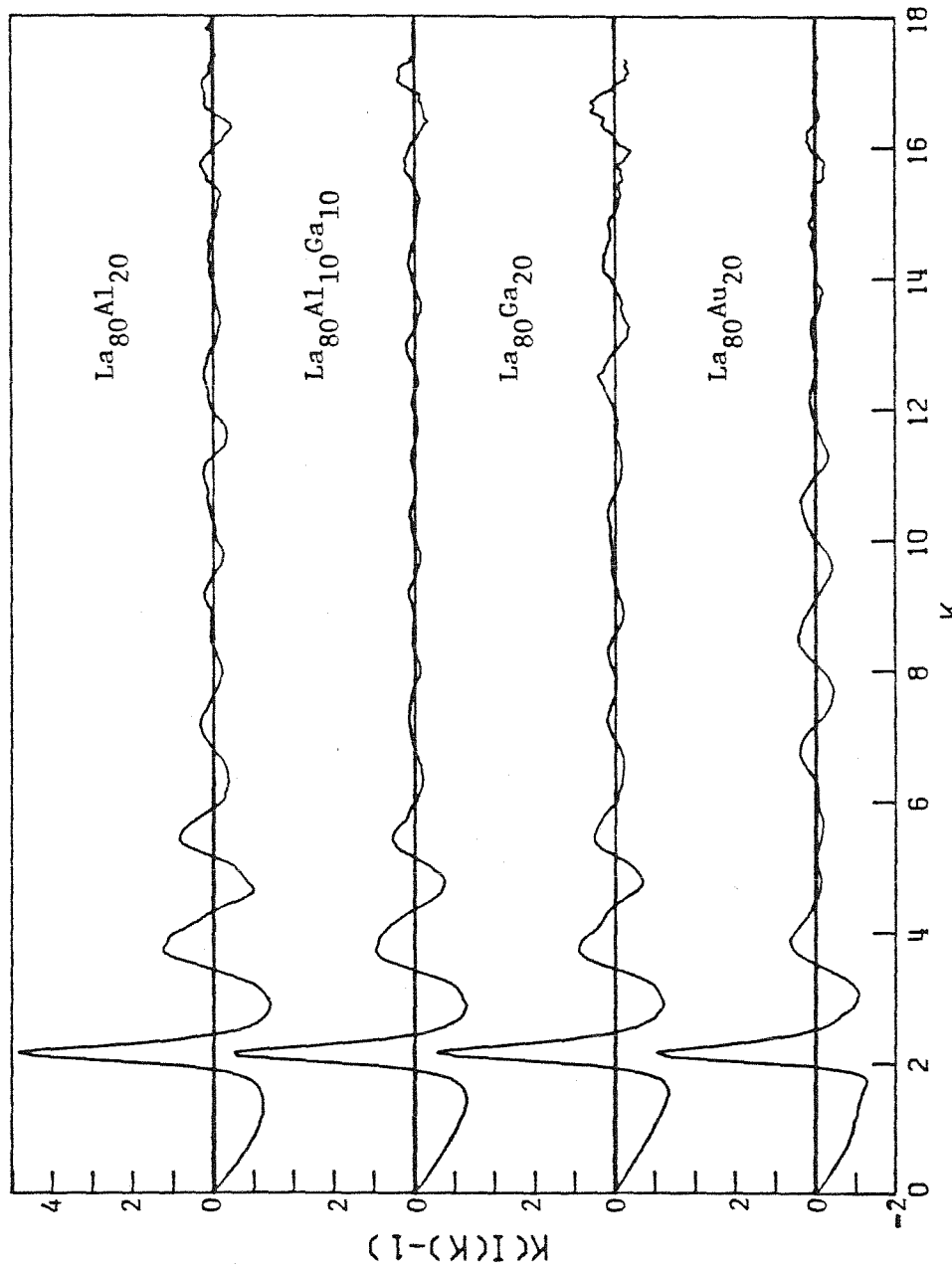

Figure 22. X-ray reduced interference functions i(K) = K(I(K)-1) for metallic glasses with 80 atomic percent lanthanum.

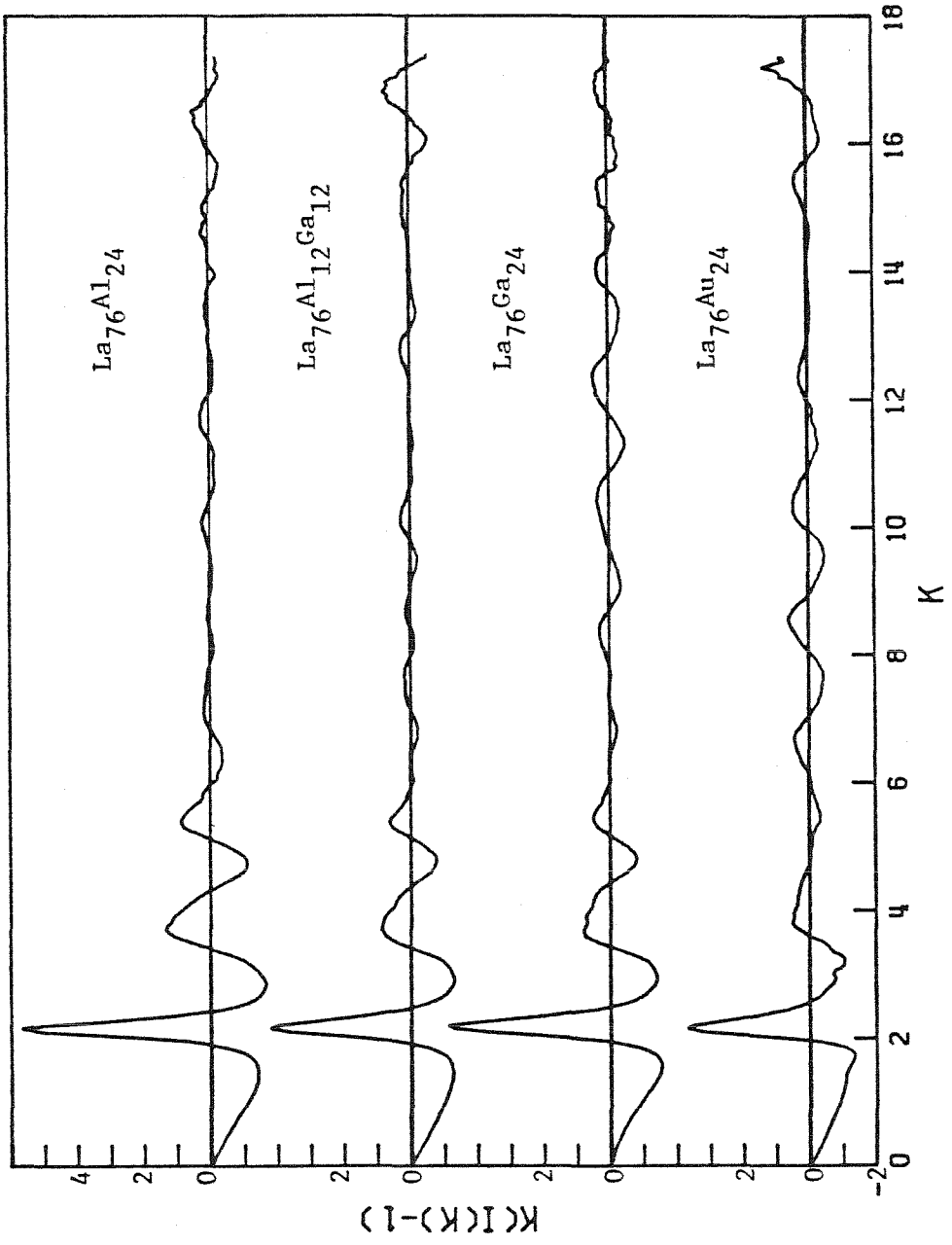

Figure 23. X-ray reduced interference functions i(K) = K(I(K)-1) for metallic glasses with 76 atomic percent lanthanum.

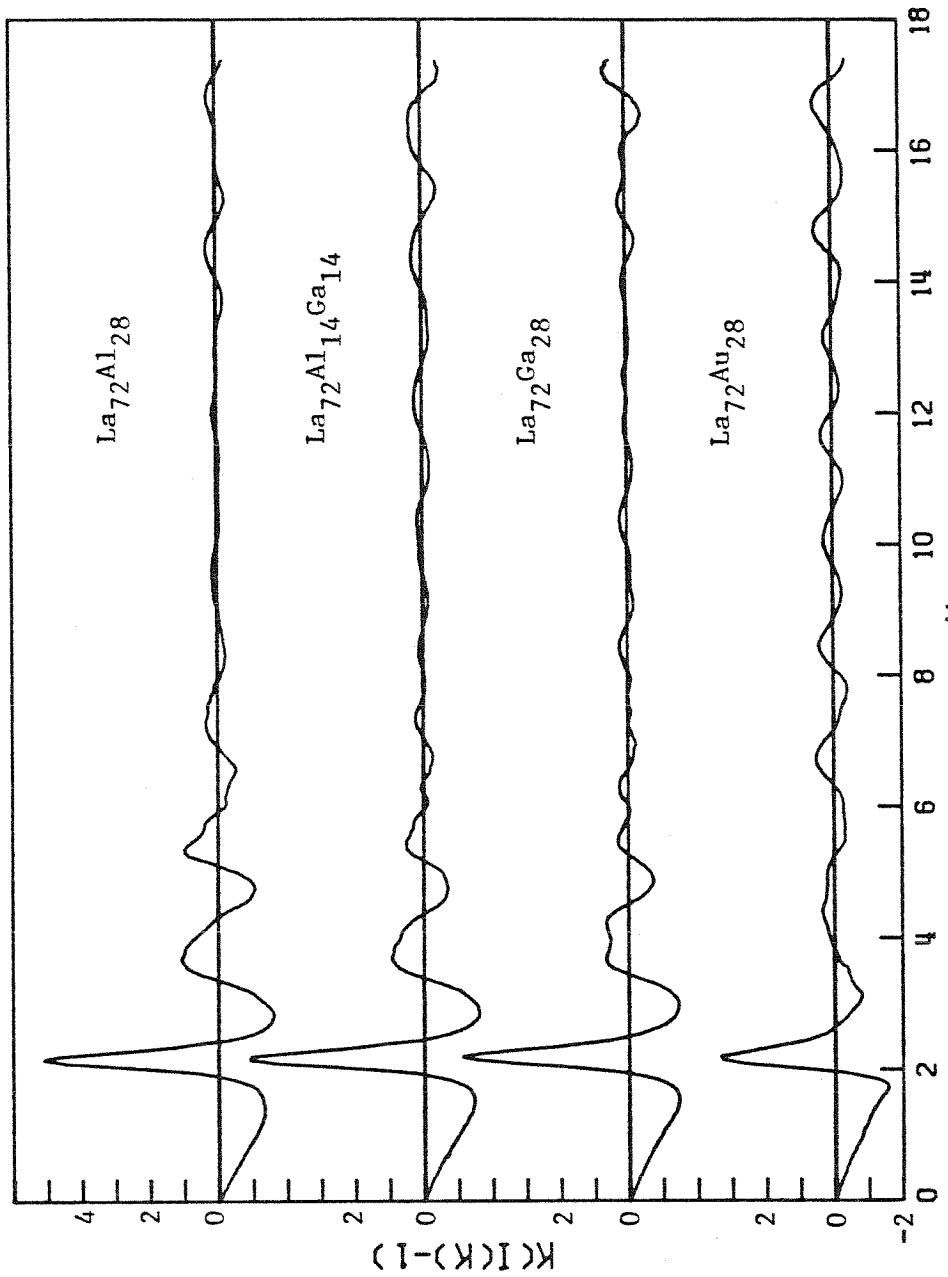

Figure 24. X-ray reduced interference functions i(K) = K(I(K)-1) for metallic glasses with 72 atomic percent lanthanum.

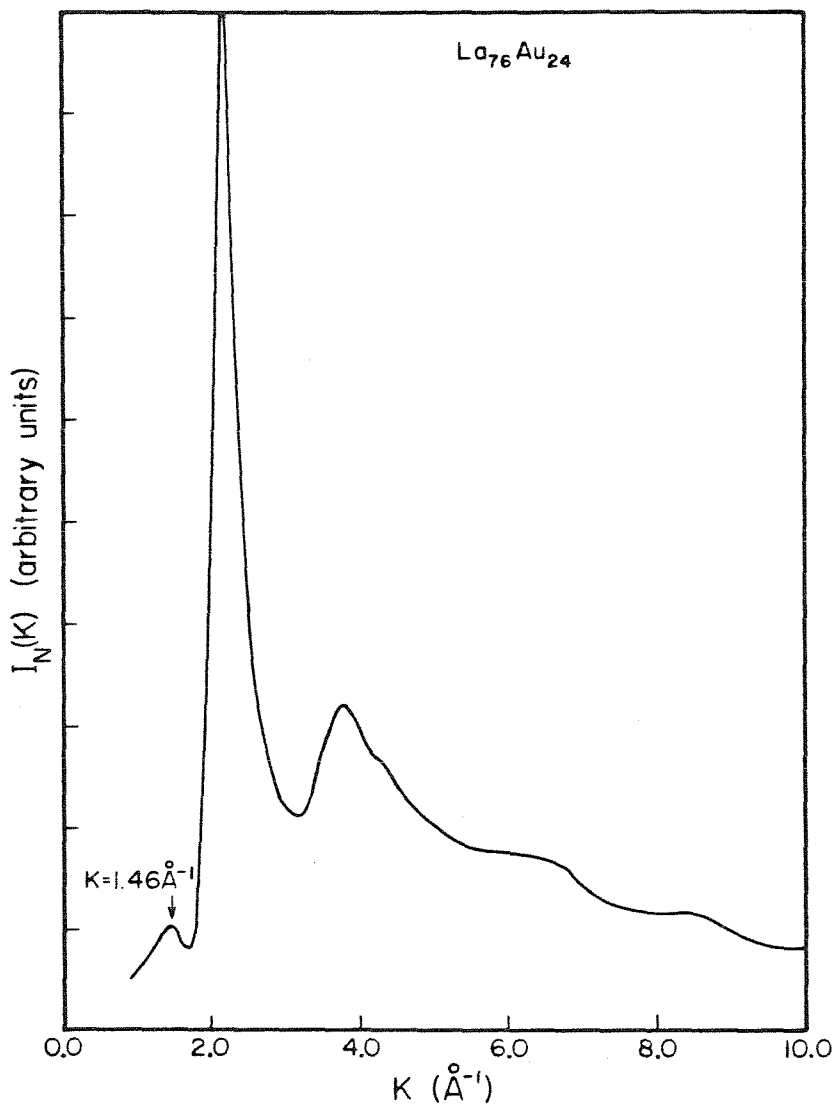

Figure 25. X-ray coherent scattering intensity, $I_N(K)$, of the metallic glass $La_{76}Au_{24}$, displaying prepeak at K = 1.46 Å^{-1}.

$La_{76}Ga_{24}$ and possibly for $La_{72}Al_{14}Ga_{14}$ and $La_{80}Ga_{20}$, these features are much smaller and less distinct than in the La-Au alloys. The prepeak definitely reflects a part of the amorphous structure and not a microcrystalline inclusion since the feature completely disappears along with the main diffraction band upon crystallization of the sample. The ratio of the prepeak height to the height of the main diffraction maximum is approximately equal to 0.08, 0.10, and 0.17 for $La_{80}Au_{20}$, $La_{76}Au_{24}$, and $La_{72}Au_{28}$ respectively, and from table (I), the corresponding ratios $W_{Au-Au}/(W_{La-La} + W_{La-Au} + W_{Au-La})$ are 0.071, 0.10, and 0.14. It seems very likely, therefore, that the prepeaks are the diffraction maxima associated with a Au-Au correlation length. From the position of the prepeaks (~1.5 $\mathring{A}^{-1}$) an estimate of this distance using the Bragg equation, $d = 2\pi/K$, yields $d \cong 4.2$ $\mathring{A}$. The prepeaks then, correspond to pairs of Au atoms separated by a very large, but highly correlated distance. Unfortunately, however, no peak at this distance is visible in the G(r) for $La_{1-x}Au_x$, since the prepeak, already small in $I_N(K)$, becomes almost insignificant in the reduced interference function,

$$i(K) = K\left[\frac{I_N(K) - \langle|f|^2\rangle}{|\langle f\rangle|^2}\right].$$

The total reduced radial distribution functions obtained for the twelve alloys studied are shown in figures (26) through (28). Although the second bands are assymmetrical, only those for $La_{80}Al_{20}$ and $La_{80}Al_{10}Ga_{10}$ are actually split as in TM-M alloys, and then only weakly. The primary maxima of the G(r)s of the non-gold alloys correspond mostly only to La-La nearest neighbors, but the increasing contributions from La-M, (M = Al,Ga), neighbors can be seen in the progressively

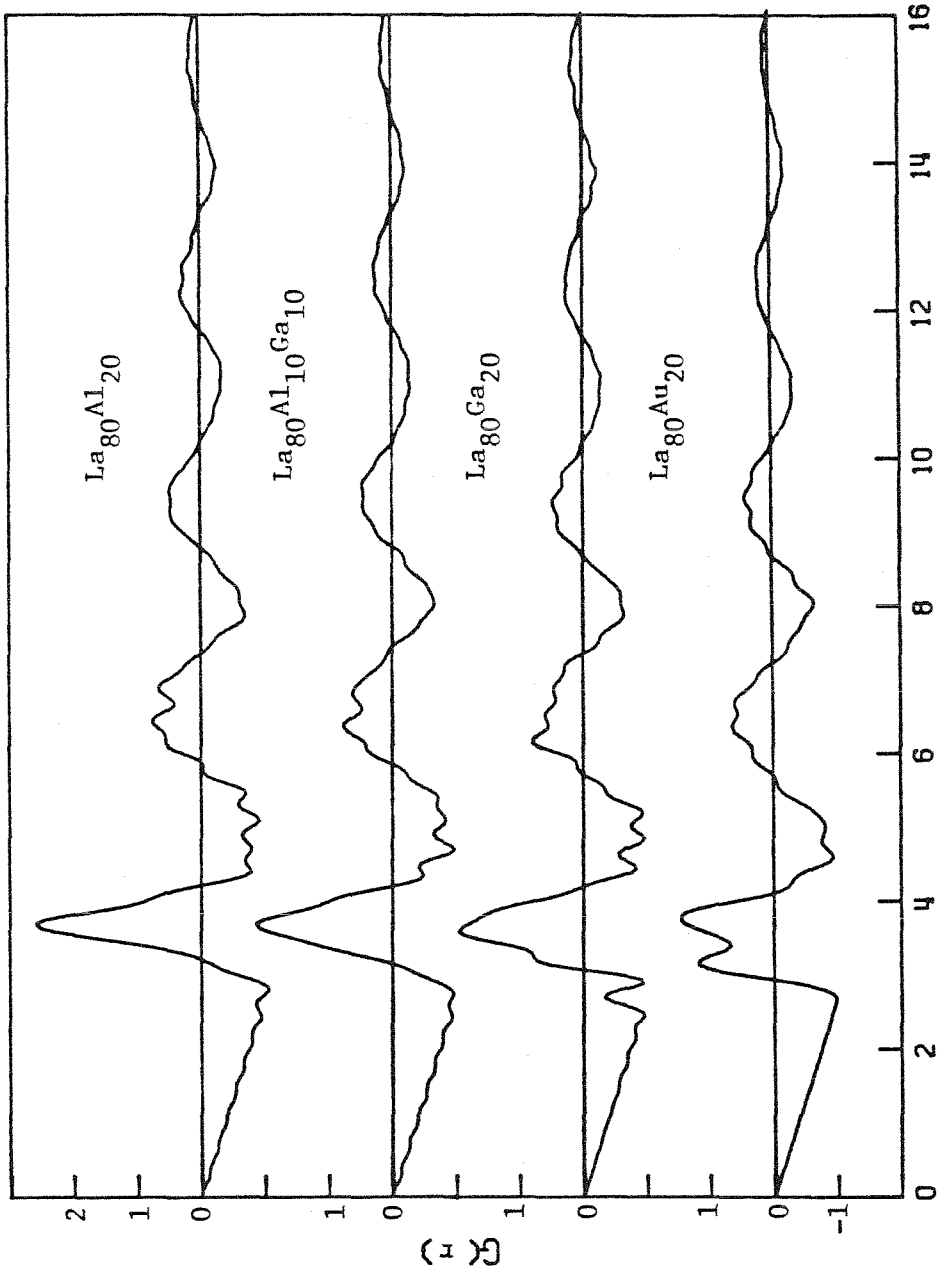

Figure 26. Total reduced radial distribution functions G(r) for metallic glasses with 80 atomic percent lanthanum, computed with a convergence factor exp(-0.002 K^2).

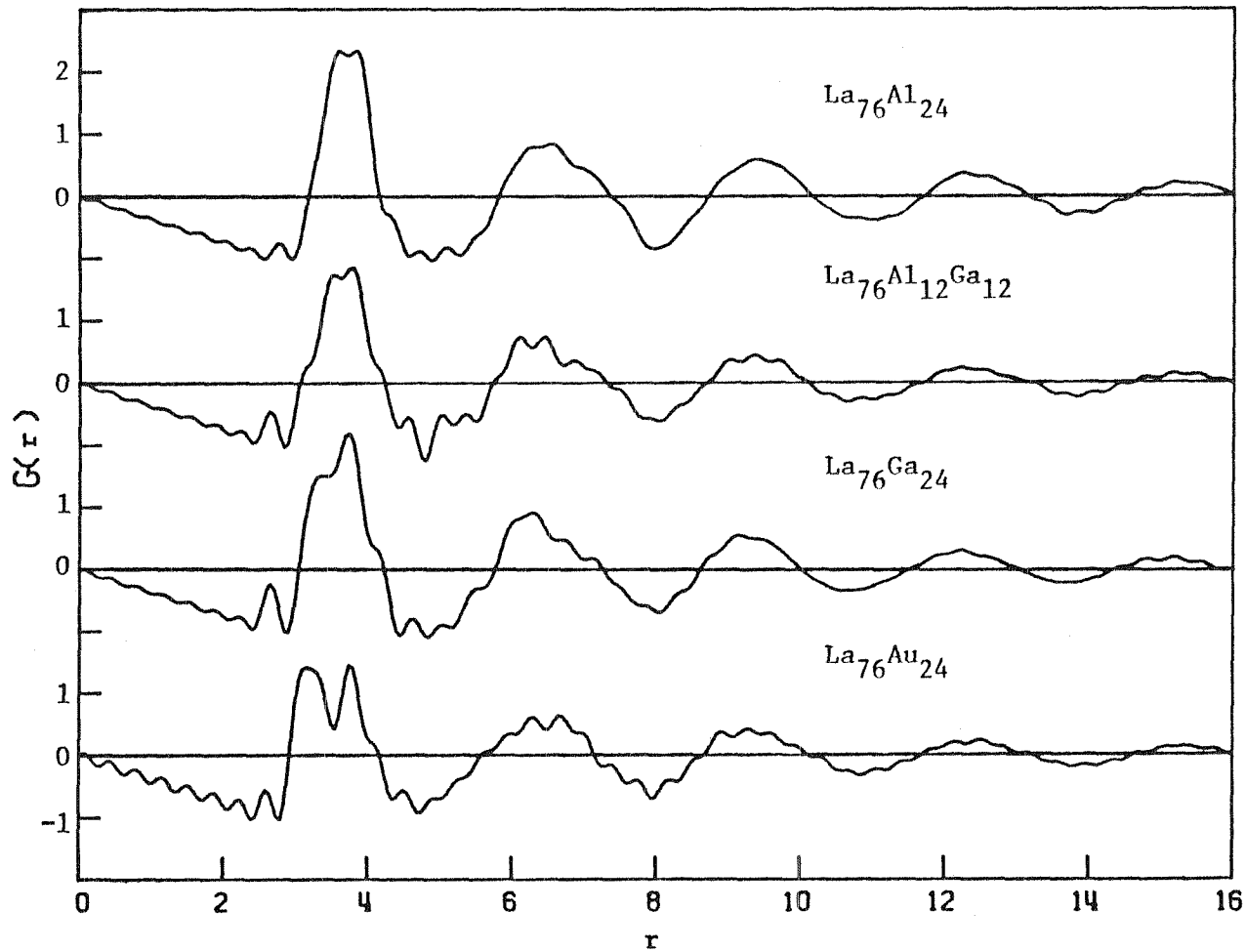

Figure 27. Total reduced radial distribution functions G(r) for metallic glasses with 76 atomic percent lanthanum, computed with a convergence factor $\exp(-0.002\ K^2)$.

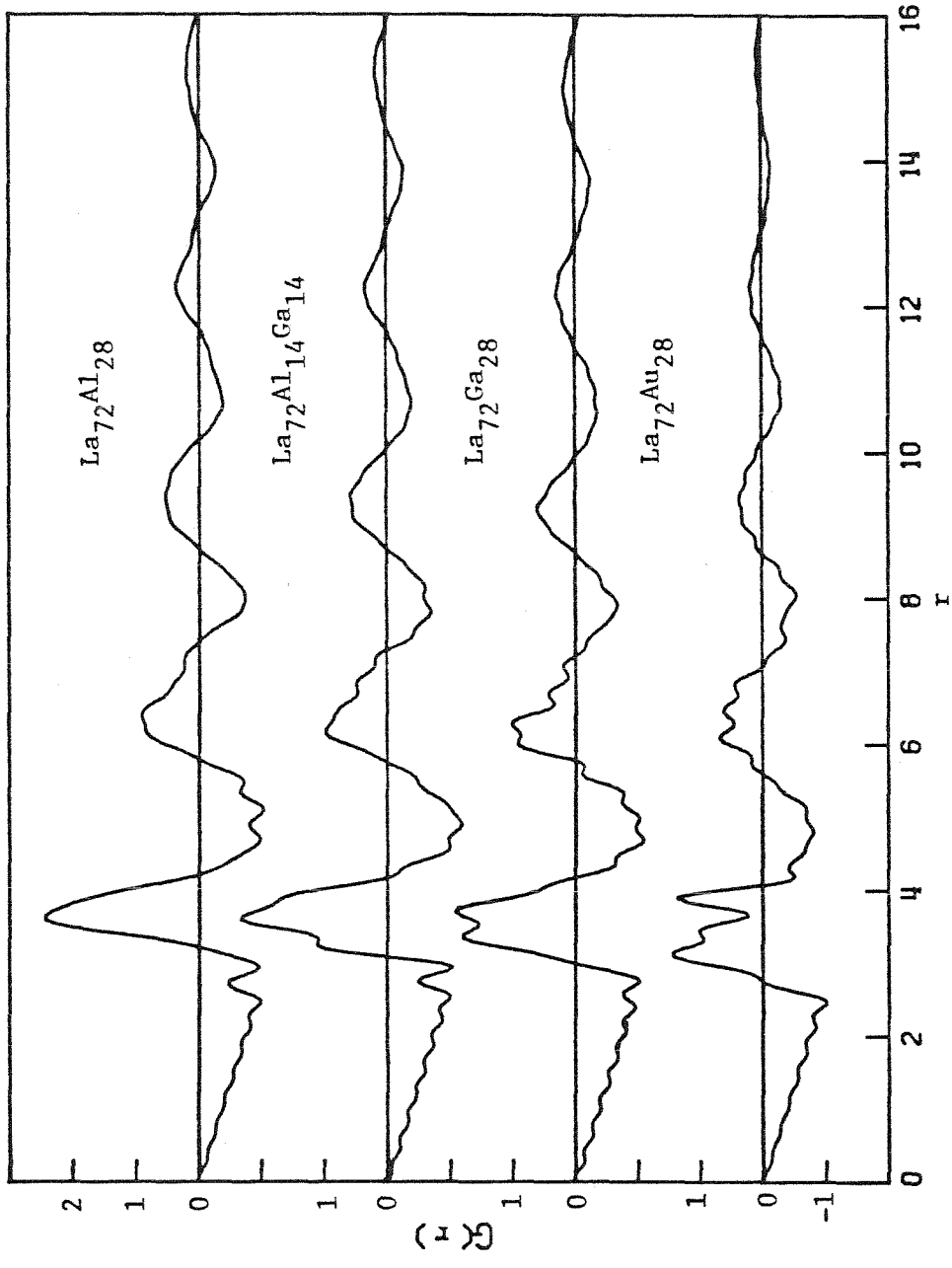

Figure 28. Total reduced radial distribution functions G(r) for metallic glasses with 72 atomic percent lanthanum, computed with a convergence factor $\exp(-0.002\ K^2)$.

more assymmetric primary bands of the La-Al, La-Al-Ga, and La-Ga distribution functions. In the La-Au alloys, where contributions from La-La and La-Au pairs are comparable, the primary band of G(r) is split. The second peak of $La_{80}Au_{20}$, for example, gives a La-La distance of about 3.78 Å, or a La radius of 1.87 Å, which is equal to the Goldschmidt radius of La. The first peak in G(r) gives a La-Au distance of 3.20 Å, or a Au radius of 1.33 Å, close to the covalent radius of Au.

For all the alloys investigated, the value of R_2/R_1, (or correspondingly, R_3/R_2 for La-Au) is about 1.73, very close to the DRPHS value. Uncharacteristic, however, of both the DRPHS and most amorphous TM-M alloys, no trace of a peak is evident near $2R_1$.

The similarity of the reduced radial distribution functions of $La_{1-x}Al_x$ and $La_{1-x}Ga_x$ suggests that these metallic glasses are isostructural, with Al and Ga performing identical roles in the structure. This is not unreasonable since Al and Ga are isoelectronic simple metals with similar electronegativities and atomic radii and form similar intermetallic compounds with La, (LaAl, LaGa are orthorhombic CaSi type structure; La_3Al, La_3Ga are cubic Cu_3Au [59]). Density measurements performed on all the alloys studied are nearly identical for each group of four alloys with given lanthanum concentration. Table (VI) lists the densities, along with some of the peak positions of the G(r)s shown in figures (26) - (28).

With the definition of a partial interference function,

$$i_{ij}(K) = \int_0^\infty 4\pi r\left[\rho_{ij}(r)/C_j - \rho_0\right] \sin(Kr)dr$$

Alloy	R_1(Å) ±.02 Å	R_2(Å) ±.03 Å	R_2/R_1 ±.02	R_3/R_1 ±.03	R_3/R_2 ±.05	ρ_0(atoms / Å^3) ±.0003
$La_{80}Al_{20}$	3.68	6.40	1.74	1.87	-	0.02909
$La_{80}Al_{10}Ga_{10}$	3.67	6.36	1.73	1.85	-	0.02966
$La_{80}Ga_{20}$	3.61	6.21	1.72	-	-	0.03018
$La_{80}Au_{20}$	3.20	3.74	-	-	1.71	0.02945
$La_{76}Al_{24}$	3.66	6.42	1.75	-	-	0.03071
$La_{76}Al_{12}Ga_{12}$	3.64	6.21	1.71	-	-	0.03083
$La_{76}Ga_{24}$	3.69	6.23	1.69	-	-	0.03098
$La_{76}Au_{24}$	3.19	3.76	-	-	1.70	0.3001
$La_{72}Al_{28}$	3.64	6.32	1.74	-	-	0.03109
$La_{72}Al_{14}Ga_{14}$	3.62	6.21	1.72	-	-	0.03133
$La_{72}Ga_{28}$	3.51	6.19	1.76	-	-	0.03147
$La_{72}Au_{28}$	3.14	3.86	-	-	1.66	0.03053

Table VI. Atomic densities and first, second, and third maxima in the atomic density functions $\rho(r)$ for the 12 lanthanum based metallic glasses.

the total reduced interference function for an experiment α, with scattering factors $f^{(\alpha)}(K)$, on an alloy with compositions C_i can be written as

$$i^{(\alpha)}(K) = \sum_{i,j} W_{ij}{}^{(\alpha)}(K)\, i_{ij}(K)$$

with the usual definition for $W_{ij}{}^{(\alpha)}(K)$

$$W_{ij}{}^{(\alpha)}(K) = \frac{C_i C_j f_i{}^{(\alpha)}(K) f_j{}^{(\alpha)}(\overset{*}{K})}{|\langle f^{(\alpha)}(K)\rangle|^2}$$

For a binary alloy, three independent experiments, (different $W_{ij}{}^{(\alpha)}(K)$), are sufficient to uniquely determine i_{11}, i_{12}, and i_{22}. For a ternary alloy system with atomic concentrations C_1, C_2, C_3, in which type 2 and type 3 atoms completely and randomly substitute for each other in the structure of the material we have $\rho_{i2}(r)/C_2 = \rho_{i3}(r)/C_3$ and consequently $i_{i2} = i_{i3}$. Along with the usual relation $i_{ij} = i_{ji}$, the total reduced interference function for such a substitutionally disordered ternary alloy can be written as

$$i = |\langle f\rangle|^{-2} \cdot \Big[C_1^2 |f_1|^2 i_{11} + 2C_1C_2\mathrm{Re}(f_1 f_2^*) i_{12} + 2C_1C_3\mathrm{Re}(f_1 f_3^*) i_{13}$$
$$+ C_2^2 |f_2|^2 i_{22} + 2C_2C_3\mathrm{Re}(f_2 f_3^*) i_{23} + C_3^2 |f_3|^2 i_{33} \Big]$$
$$= |\langle f\rangle|^{-2} \cdot \left[C_1^2 |f_1|^2 i_{11} + 2C_1(C_2+C_3)\mathrm{Re}\left\{ f_1 \cdot \left(\frac{C_2 f_2 + C_3 f_3}{C_2+C_3} \right)^* \right\} i_{12} \right.$$
$$\left. + (C_2+C_3)^2 \left| \frac{C_2 f_2 + C_3 f_3}{C_2+C_3} \right|^2 i_{22} \right]$$

The scattered intensity is exactly the same as for a binary alloy composed only of element 1 plus some element whose atomic form factor equals the compositional average of f_2 and f_3. In principal, then, if Al and Ga substitute randomly in amorphous La-Al-Ga alloys then the three X-ray diffraction patterns for $La_{1-x}Al_x$, $La_{1-x}(Al\text{-}Ga)_x$ and $La_{1-x}Ga_x$ provide sufficient information to extract the three independent partial interference functions $i_{La-La}(K)$, $i_{La-M}(K)$ and $i_{M-M}(K)$, (where M = Al,Ga), by the solution of

$$\begin{pmatrix} i_{La-La} \\ i_{La-M} \\ i_{M-M} \end{pmatrix} = \begin{pmatrix} W_{La-La}^{(La-Al)} & W_{La-M}^{(La-Al)} & W_{M-M}^{(La-Al)} \\ W_{La-La}^{(La-Al-Ga)} & W_{La-M}^{(La-Al-Ga)} & W_{M-M}^{(La-Al-Ga)} \\ W_{La-La}^{(La-Ga)} & W_{La-M}^{(La-Ga)} & W_{M-M}^{(La-Ga)} \end{pmatrix}^{-1} \begin{pmatrix} i(La-Al) \\ i(La-Al-Ga) \\ i(La-Ga) \end{pmatrix} \quad (4)$$

from which the $\rho_{La-La}(r)$, $\rho_{La-M}(r)$ and $\rho_{M-M}(r)$ can be obtained.

Since the elements of the matrix of coefficients above are of different orders of magnitude, ($W_{La-La}^{(La_{80}Al_{20})} = 0.895$, $W_{Al-Al}^{(La_{80}Al_{20})} = 0.0029$ from table (I)), a small error in f(K) or i(K) can be amplified into a disastrously large error in the $i_{ij}(K)$. It was therefore necessary first to minimize errors in the i(K) due to incorrect accounting for background, errors in the computed f(K) and errors in normalization. This was done by noting that upon computing the sine transform of i(K)

plus a small, slowly varying error function $\varepsilon(K)$, a very noticeable effect in the behavior of $G(r)$ at small r occurs even for small $\varepsilon(K)$. (70)

$$\int_0^{K_{max}} [i(K) + \varepsilon(K)] \sin(Kr)dK$$

$$\cong 4\pi r\,[\rho(r) - \rho_0] + \langle\varepsilon(K)\rangle \frac{2\sin^2(K_{max}r)}{r}$$

Since for small r, $G(r) = 4\pi\rho_0 r$, the effect of $\varepsilon(K)$ is to introduce oscillations at small r about the otherwise straight line for $G(r)$. For $K_{max} = 17.4\ \text{Å}^{-1}$, the maximum in the oscillations will occur at about $r = 0.1$ Å. The error function $\varepsilon(K)$ was therefore determined for each $i(K)$ as an exponentially damped quartic polynomial which provided a least squares fit of the resulting sine transform of $i(K) - \varepsilon(K)$ to the straight line $-4\pi\rho_0 r$ in the region $0<r<0.5$ Å. Restricting the fit to this region prevents confusion from errors due to termination oscillations, which have a period of about 0.4 Å. The required minimization sum is

$$\text{minimize} \sum_{0<r<0.5} \left[-4\pi\rho_0 r - \int_0^{K_{max}} \left\{i(K) - e^{\alpha K^2}(aK+bK^2+cK^3+dK^4)\right\}\sin(Kr)dK\right]^2$$

with respect to the constants a,b,c, and d. The value of α used was 0.01, the exponential term $e^{-\alpha K^2}$ having been included to keep the error function well behaved at large K. The choice of a polynomial is general enough to fit a slowly varying function and keeps the least squares fitting procedure relatively simple. The zeroth order term

was excluded from the polynomial in order to preserve the condition $I(0) = 0$. The improvements in i(K) which are affected by this technique are what made possible the extraction of the partial interference functions. The error in the i(K)s shown in figures (22) - (24), which have been processed through the above technique, is estimated to be less than about 2% in the region below $K \cong 8\ \mathring{A}^{-1}$.

Table (I) shows that the greatest scattering contribution from M-M pairs, (M = Al,Ga), for the $La_{1-x}M_x$ alloys studied is about 3% of the total scattering (for $La_{72}Ga_{28}$). With an experimental uncertainty on the order of 2%, determination of $\rho_{M-M}(r)$ becomes impossible from these data. In fact, the smallness of the contribution from M-M pairs allows their contribution to be neglected in the analysis, from which $\rho_{La-La}(r)$ and $\rho_{La-M}(r)$ can still be determined from any pair of $La_{1-x}M_x$ alloys. These functions were determined for each of the three pairs of data possible, ($La_{1-x}Al_x$ - $La_{1-x}(Al\text{-}Ga)_x$, $La_{1-x}(Al\text{-}Ga)_x$ - $La_{1-x}Ga_x$, and $La_{1-x}Al_x$ - $La_{1-x}Ga_x$), for each composition x = 0.20, 0.24 and 0.28 and were found to be consistent within the experimental errors, as figures (29) and (30) show, for example, for x = 0.28. The consistency demonstrated by the results is a necessary, (although certainly not sufficient), condition for the isomorphism of $La_{1-x}Al_x$ and $La_{1-x}Ga_x$.

Included in figures (29) and (30) are $G_{La-La}(r)$ and $G_{La-M}(r)$ obtained from the complete solution of equation (4) using the data from $La_{72}Al_{28}$, $La_{72}Ga_{28}$ and $La_{72}Au_{28}$. The solution obtained is nearly identical to that calculated from $La_{72}Al_{28}$ - $La_{72}Ga_{28}$ and has a higher signal to noise ratio than any of the solutions obtained with only two sets of data by ignoring $G_{M-M}(r)$. The attempt to try the full solution for the $G_{ij}(r)$ by including La-Au was prompted by the fact that the atomic

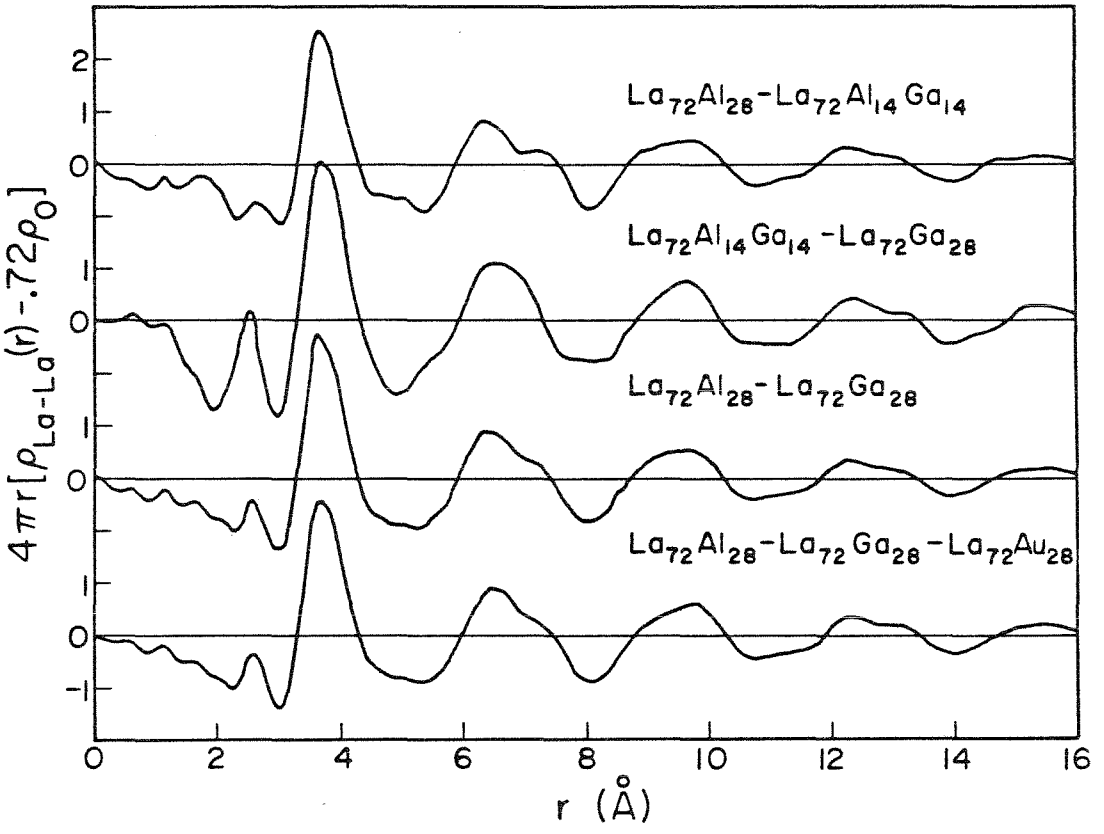

Figure 29. Partial reduced radial distribution functions, $4\pi r\,[\rho_{La-La}(r) - C_{La}\rho_0]$ computed from four different sets of data on metallic glasses with 72 atomic percent lanthanum and using a convergence factor $\exp(-0.005\ K^2)$.

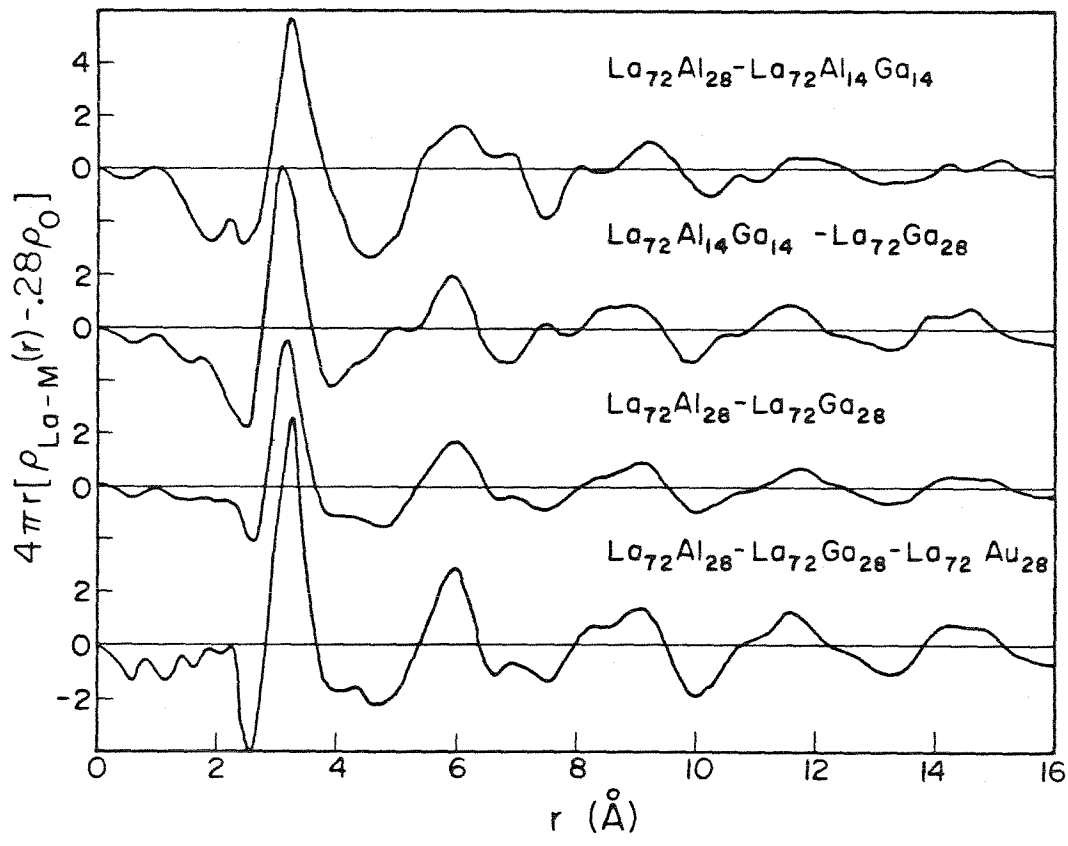

Figure 30. Partial reduced radial distribution functions, $4\pi r\,[\rho_{La-M}(r) - C_M\rho_0]$ computed from four different sets of data on $La_{72}M_{28}$ metallic glasses where M = Al, $Al_{0.5}Ga_{0.5}$, Ga, Au. A convergence factor $\exp(-0.005\ K^2)$ was used.

density of the $La_{1-x}Au_x$ metallic glasses is very close to that of $La_{1-x}Al_x$ and $La_{1-x}Ga_x$. Furthermore, the ratio $R_3/R_2 \cong 1.73$ for the amorphous La-Au, as is R_1/R_2 for La-Al and La-Ga, suggesting a similar short range order for these metallic glasses. Supporting this is the fact that for all three compositions studied, the peak positions, widths, and integrated areas determined for $\rho_{La-La}(r)$ and $\rho_{La-M}(r)$ are very nearly identical, (within 1%), for the two-fold solution with $La_{1-x}Al_x$ - $La_{1-x}Ga_x$ and the full solution using $La_{1-x}Al_x$ - $La_{1-x}Ga_x$ = $La_{1-x}Au_x$. Solutions using $La_{1-x}Al_x$ - $La_{1-x}(Al\text{-}Ga)_x$ - $La_{1-x}Au_x$ and $La_{1-x}(Al\text{-}Ga)_x$ - $La_{1-x}Ga_x$ - $La_{1-x}Au_x$, although having poorer resolution due to the poorer signal to noise ratio, also produced results which were consistent within the experimental errors. Also, Enderby et al. [41] have noted that since $I_N(K)$ is an intensity and must always be non-negative, the elementary properties of quadratic functions impose the following conditions on the components $i_{ij}(K)$ of $I_N(K)$ for a binary alloy:

$$C_1\, i_{11} > -K$$

$$C_2\, i_{22} > -K$$

$$\sqrt{C_1 C_2}\; i_{12} > -\sqrt{(K + C_1 i_{11})\,(K + C_2 i_{22})}$$

The solutions for i_{La-La}, i_{La-M}, and i_{M-M} were found to consistently satisfy these inequalities for all but a very few regions of K. It is therefore supposed that the lanthanum based metallic glasses studied here with Al, Ga, and Au are all isostructural for any particular La concentration, and figures (31) through (36) show the three independent $i_{ij}(K)$ and corresponding $G_{ij}(r)$ obtained for $La_{1-x}M_x$ for x = 0.20, 0.24, and 0.28, where now M = Al, Ga, or Au.

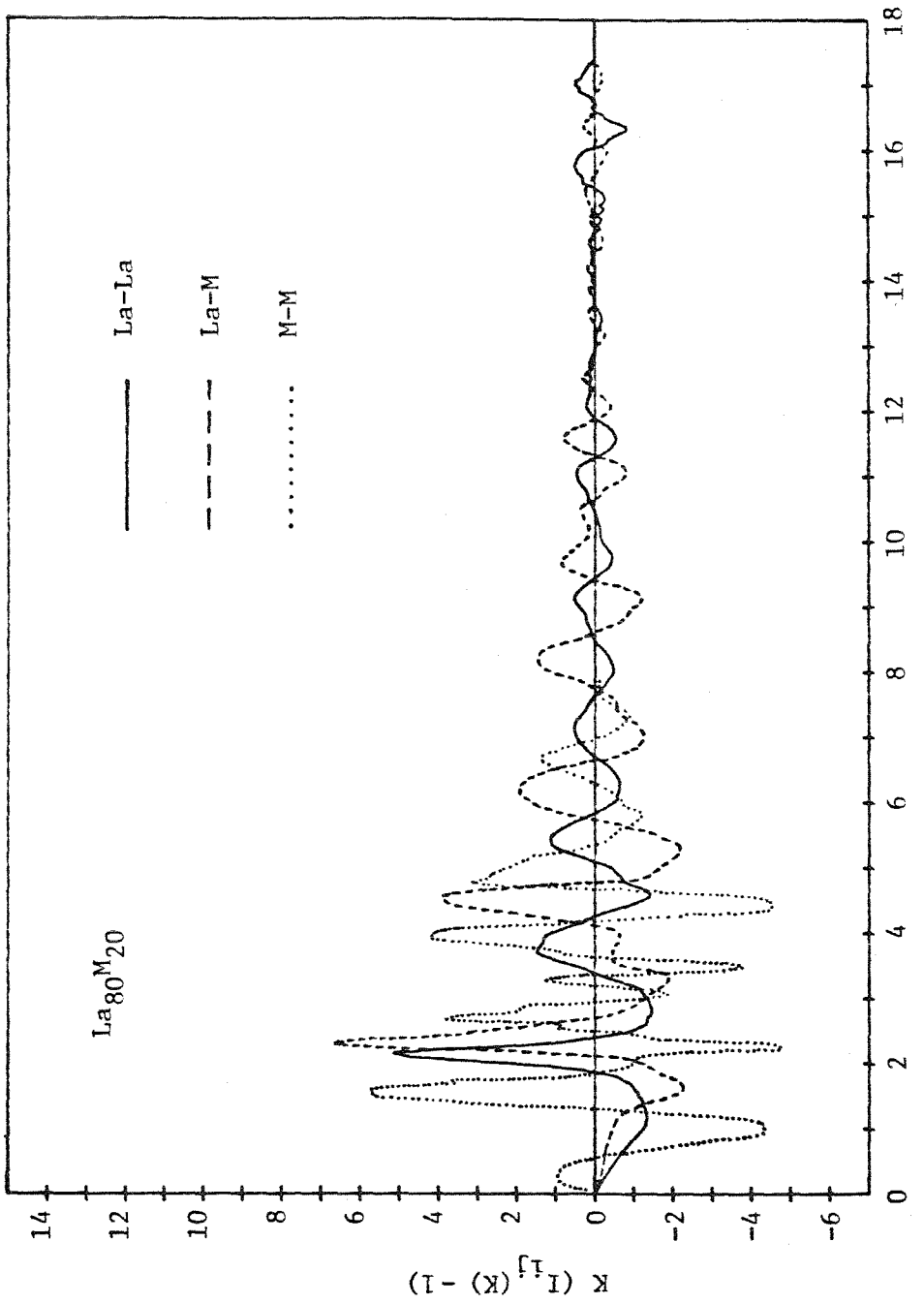

Figure 31. The three independent partial reduced interference functions $i_{ij}(K) = K(I_{ij}-1)$ for isomorphic $La_{80}Al_{20}$, $La_{80}Ga_{20}$, and $La_{80}Au_{20}$ metallic glasses.

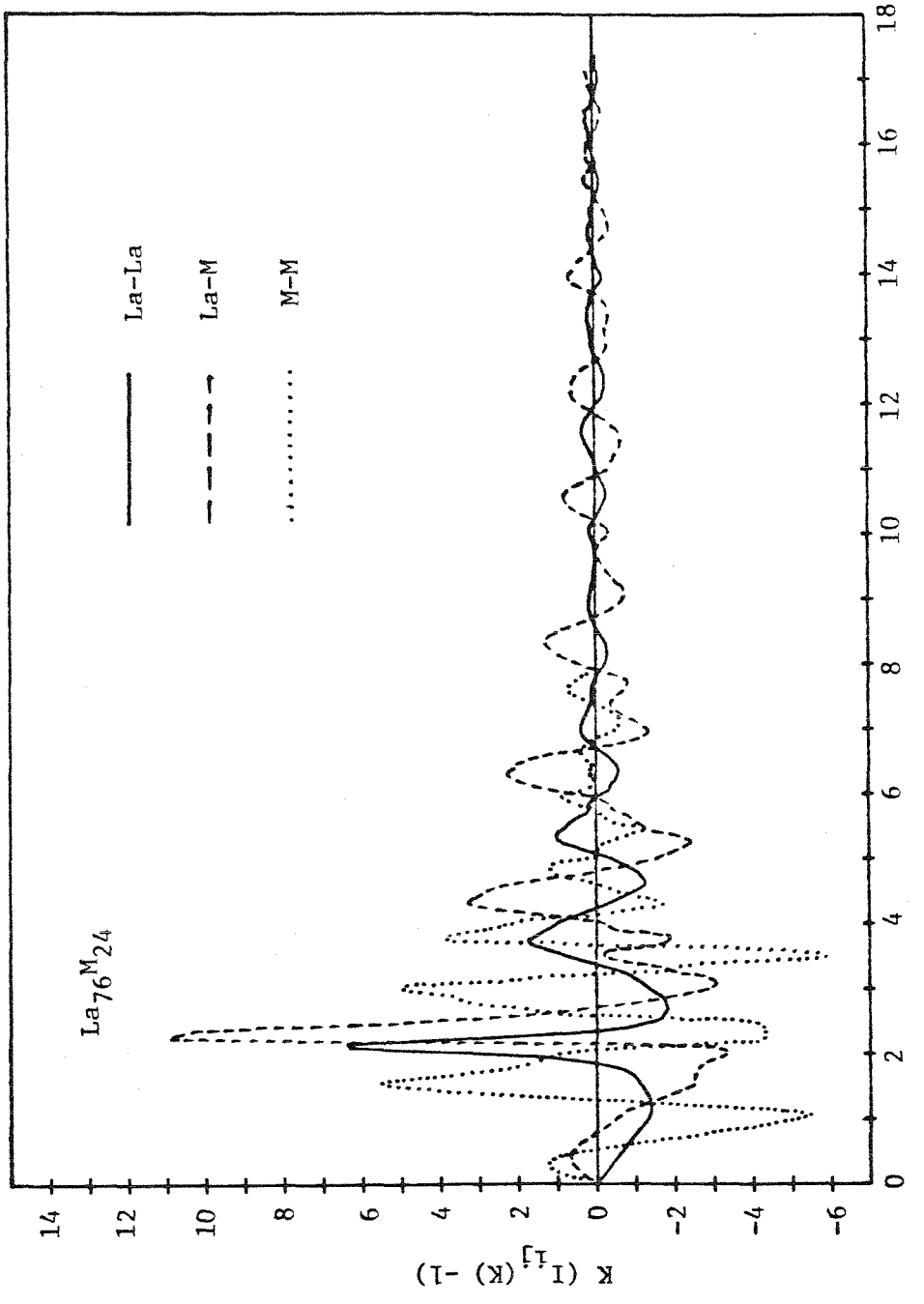

Figure 32. The three independent partial reduced interference functions $i_{ij}(K) = K(I_{ij}-1)$ for isomorphic $La_{76}Al_{24}$, $La_{76}Ga_{24}$, and $La_{76}Au_{24}$ metallic glasses.

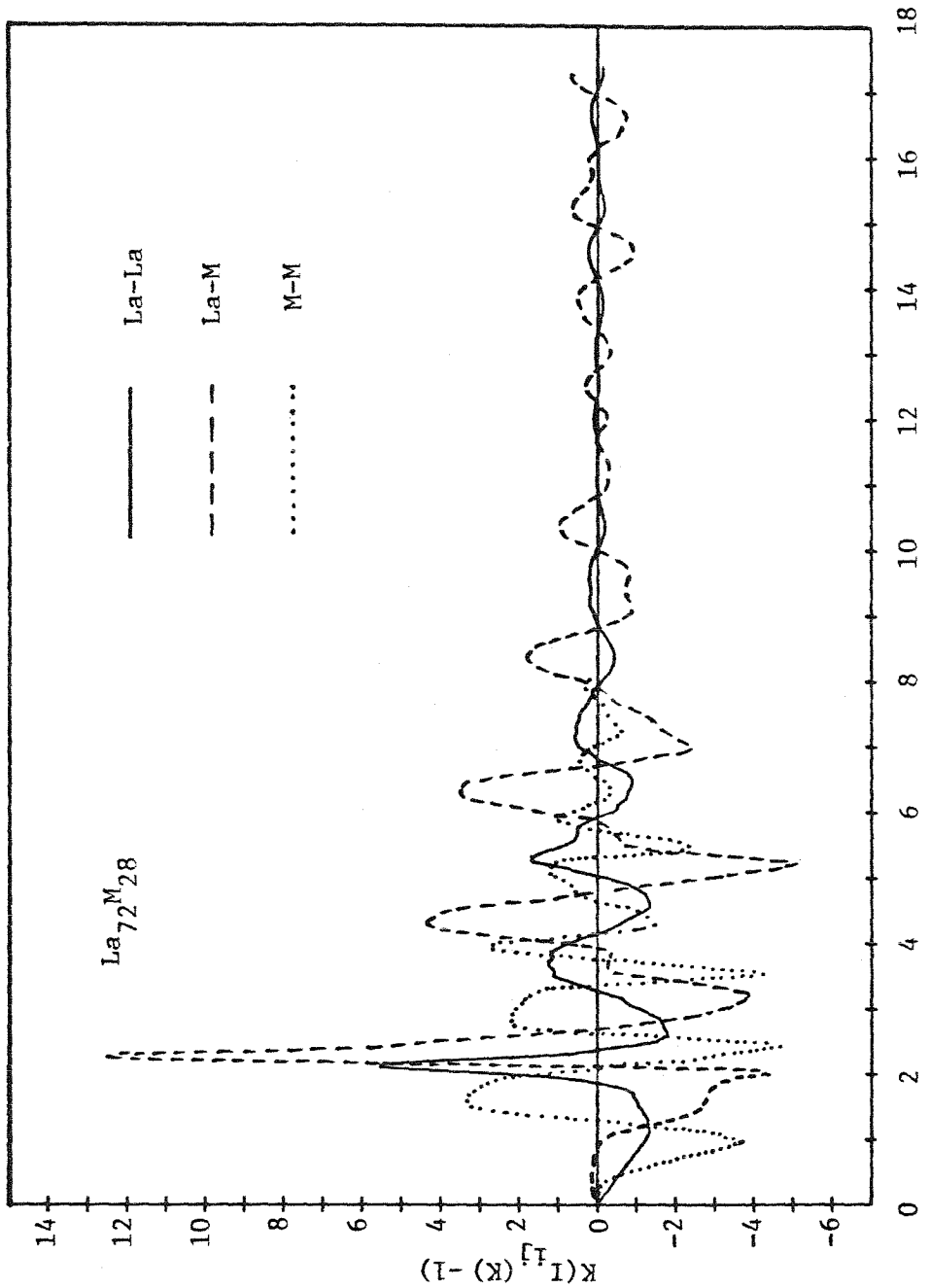

Figure 33. The three independent partial reduced interference functions $i_{ij}(K) = K(I_{ij}-1)$ for isomorphic $La_{72}Al_{28}$, $La_{72}Ga_{28}$, and $La_{72}Au_{28}$ metallic glasses.

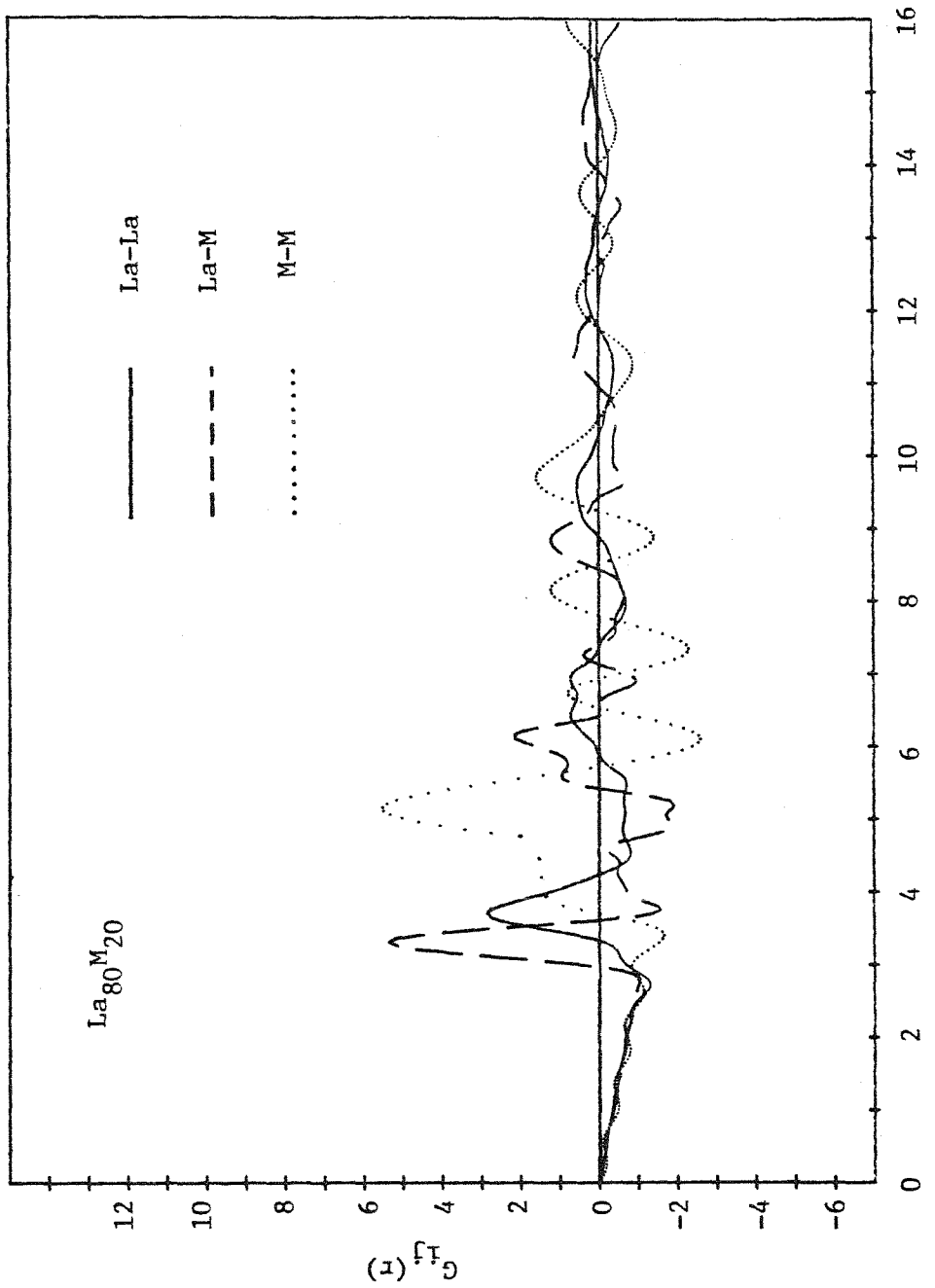

Figure 34. The three independent partial reduced radial distribution functions $G_{ij}(r)$ for isomorphic $La_{80}Al_{20}$, $La_{80}Ga_{20}$, and $La_{80}Au_{20}$ metallic glasses.

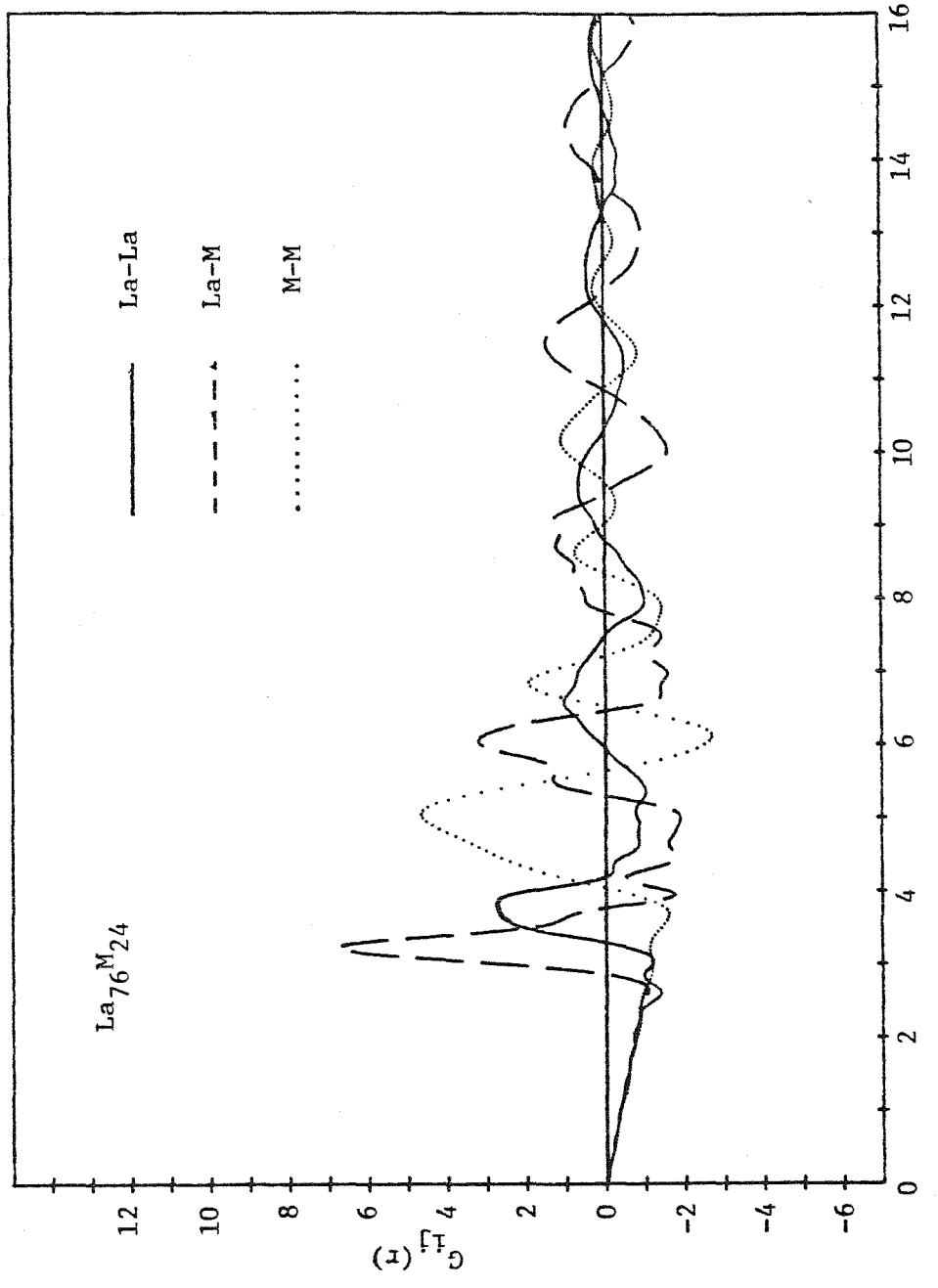

Figure 35. The three independent partial reduced radial distribution functions $G_{ij}(r)$ for isomorphic $La_{76}Al_{24}$, $La_{76}Ga_{24}$, and $La_{76}Au_{24}$ metallic glasses.

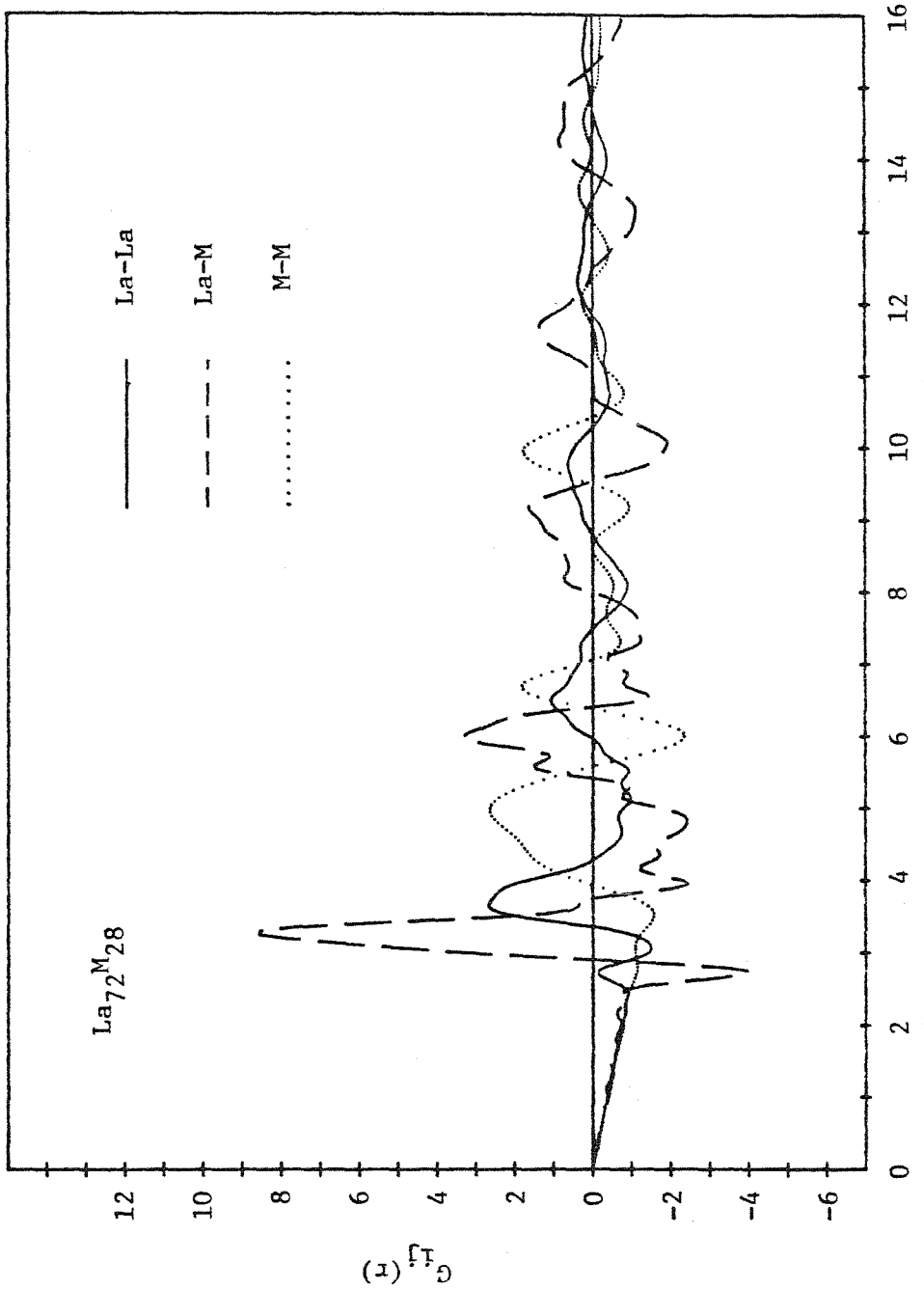

Figure 36. The three independent partial reduced radial distribution functions $G_{ij}(r)$ for isomorphic $La_{72}Al_{28}$, $La_{72}Ga_{28}$, and $La_{72}Au_{28}$ metallic glasses.

The $i_{La-La}(K)$ and $i_{La-M}(K)$ shown in figures (31) through (33) have been multiplied by an exponential convergence factor, $\exp(-.005\ K^2)$, and have been smoothed above $K = 10\ \mathring{A}^{-1}$. $i_{M-M}(K)$, being the smallest of the three components in the total intensity, (~7% in $La_{80}Au_{20}$), has the poorest signal to noise ratio and is therefore the hardest to resolve, especially at the higher lanthanum concentrations. i_{M-M} was therefore cut off at about $K = 8\ \mathring{A}^{-1}$, since essentially nothing but noise was accessible beyond this point, and a large convergence factor, $\exp(-.015\ K^2)$, was applied. The broadening in the transform of $i_{M-M}(K)$ caused by this termination and exponential damping is in fact smaller than for i_{La-La} and i_{La-M}, ($.015 \cdot 8^2 = .96$, while $.005 \cdot 17.4^2 = 1.51$). The most distinct feature of $i_{M-M}(K)$ for all three sets of metallic glasses is a rather broad primary maximum at very small wavenumber, ($1 < K < 2$), which is produced by the previously noted prepeaks in $I_N(K)$ for $La_{1-x}Au_x$. In fact the $i_{M-M}(K)$, (and $G_{M-M}(r)$), are actually representative only of Au-Au pairs since Al and Ga make only insignificant contributions to the extracted pair intensity function. It is not really fair then to refer to M-M pairs collectively as Al, Ga, Au since we only have the data for Au, and this should be kept in mind.

In all three alloy groups the M-M pair correlation functions have only a single distinct, broad, maximum between 5 and 6 Angstroms. A pair of Au atoms are therefore very seldom, if ever, near neighbors in these metallic glasses. This type of clear chemical ordering has been observed in several amorphous TM-M alloys such as electrodeposited $Co_{81}P_{19}$, [42] sputtered $Pd_{80}Ge_{20}$, [9] and liquid quenched $Pd_{84}Si_{16}$ [71] and $Pd_{78}Ge_{22}$. [9]

Table (VII) shows the coordination numbers and positions and widths of the primary maxima of the pair density functions, $\rho_{ij}(r)$, for the three groups of $La_{1-x}M_x$ metallic glasses studied. Data are also included for crystalline La_3Al and for amorphous $Co_{81}P_{19}$,[42] $Pd_{80}Ge_{20}$[9] and $Pd_{84}Si_{16}$.[17] Coordination numbers were obtained from integration of $4\pi r^2 \rho_{ij}(r)$ to the minimum following the primary peak in the pair density function, and band widths listed are FWHM of $\rho_{ij}(r)$ corrected for convergence and termination broadening effects.

From Table (VII) the average La-La nearest neighbor distance for the $La_{1-x}M_x$ metallic glasses is just twice the La Goldschmidt radius, 1.87 Å. The total La coordination is close to 12, that of the pure metal and of the intermetallic compound $La_3(Al\text{-}Ga)$, and increases with increasing x at about 0.2 atoms per % M. The La-La coordination number changes little with composition, (no trend is visible at least within the resolution of the experiment), in agreement with computer models of binary DRP models,[72,73] and both the observed $n_{La\text{-}La}$ and $n_{La\text{-}M}$ are little different from those expected from a completely disordered alloy. Using $(1\text{-}x)n_{La}$ as the La-La and xn_{La} as the La-M coordinations for a disordered $La_{1-x}M_x$ alloy yields $n_{La\text{-}La}$ = 9.22, 9.80, and 9.57 and $n_{La\text{-}M}$ = 2.30, 3.09, and 3.72 for x = 0.20, 0.24, and 0.28 respectively, all very close to the coordination numbers observed for the metallic glasses. The M-atom coordinations, on the other hand, show distinct signs of strong chemical ordering. Using $(1\text{-}x)n_{M\text{-}La}$ and $xn_{M\text{-}La}$, (since there were no M-M nearest neighbors observed), again as the expected coordinations for a completely disordered alloy yields $n_{M\text{-}La}$ = 6.24, 7.34, and 6.94, and $n_{M\text{-}M}$ = 1.56, 2.32, and 2.70. The fact that no M-M nearest neighbors were found, (or at least, considerably < 1), even for $La_{72}M_{28}$ which has the largest

Alloy	R_{La-La} (±0.04Å)	R_{La-M} (±0.05Å)	R_{M-M} (±0.2Å)	ΔR_{La-La} (±0.01Å)	ΔR_{La-M} (±0.01Å)	ΔR_{M-M} (±0.1Å)	η_{La-La} (±0.7)	η_{La-M} (±0.2)	η_{La} (±0.9)	η_{M-La} (±0.9)	η_{M-M} (±1.5)
$La_{80}M_{20}$	3.73	3.27	5.11	0.43	0.14	0.51	9.57	1.95	11.52	7.80	8.09
$La_{76}M_{24}$	3.75	3.22	5.02	0.49	0.15	1.02	9.84	3.05	12.89	9.66	9.28
$La_{72}M_{28}$	3.71	3.25	4.94	0.49	0.16	1.23	9.54	3.75	13.29	9.64	8.60
La_3Al [59]	3.60	3.60	5.093	-	-	-	8	4	12	8	6
$Co_{81}P_{19}$ [42]	2.55	2.32	3.34	0.43	0.33	0.70	10.1	2.09	12.19	8.9	-
$Pd_{80}Ge_{20}$ [9]	-	2.49	-	-	0.20	-	-	2.15	-	8.6	-
$Pd_{84}Si_{16}$ [9]	2.78	2.40	-	-	-	-	-	1.71	-	9.0	-

Table VII. First maxima positions of the atomic density functions, $\rho_{ij}(r)$ and their full widths at half maximum and coordination numbers for several amorphous alloys and for crystalline La_3Al.

expected n_{M-M} and the highest experimental signal to noise ratio is strong evidence for chemical ordering in these materials.

The La-M nearest neighbor distance is observed to be considerably smaller than the sum of the metallic radii of the two atoms. Using $R_{La-M} - \frac{1}{2}R_{La-La}$ to evaluate the M atom size in the matrix produces an average value of $\simeq$ 1.38 Å $\pm$ 0.03 Å for the three groups of alloys, which is somewhere between the metallic and covalent radii of Al-Ga-Au. In fact, the sharpness of the primary maximum of $G_{La-M}(r)$ and the closeness of the La-M nearest neighbors demonstrates a rather well defined La-M bond length in the metallic glass. Clustering of La atoms about M-type atoms probably establishes a local energy minimization through a charge transfer from the valence band of Al-Ga-Au (which have filled d-shells) to the partially filled d-band of La.

Crystalline La_3Al has an FCC structure with Al on the cubic lattice and La occupying the faces of the cube. No Al-Al near neighbors exist in this structure, and the coordination numbers shown in Table VII are not too different from those of the compositionally close metallic glasses, $La_{76}M_{24}$. Also, the atomic density of La_3Al, computed from the lattice parameter, is 0.03028 atoms/Å^3, nearly identical to that of the metallic glasses. In crystalline La_3Al however, Al atoms reside in very large octahedral holes in a very compressed La matrix, and the La-La and La-Al nearest neighbor separations are therefore very different from those in the metallic glasses.

The $G_{La-La}(r)$ in figures (34), (35), and (36) have second maxima at R_2/R_1 = 1.73, 1.75, and 1.74 respectively for $La_{80}M_{20}$, $La_{76}M_{24}$, and $La_{72}M_{28}$. These are all very close to $\sqrt{3}$, the position occurring in the DRPHS. No peak at all occurs near $2R_1$ however, and in fact only $La_{80}M_{20}$

has a split second maximum, the second subpeak occurring at $r \simeq 6.91$ Å, which is close to the sum of R_{La-La} and R_{La-M}, suggesting La-M-La collineations, rather than La-La-La collineations. The complete absence of La-La-La collineations precludes the occurrence of any long Bernal pseudonuclei in this structure.

The second peak in $G_{La-M}(r)$, $r \simeq 6.5$ Å, is about equal in each case to the separation of La and M atoms on opposite sides of a tetrahedral base of La atoms. A similar configuration explains the only observed maximum in $G_{M-M}(r)$. These types of configurations, opposite vertices of tetrahedra sharing a common base, as mentioned before, occur as second atoms on the pentagonal rings of the icosohedron, (figure 18)), whose 5-fold symmetry properties preclude the formation of a regular crystal structure based on icosohedra alone. A transition metal-metalloid-like structure based on icosohedral clusters however is already precluded by the complete absence of traces of the pentagonal ring configuration in $G_{La-La}(r)$, (i.e., no maxima of 1.63 R_1 or 2.0 R_1).

The short range order of the $La_{1-x}(Al\text{-}Ga\text{-}Au)_x$ metallic glasses is quite different from that of more typical amorphous TM-M alloys based on distorted icosohedral clusters. Although a strong chemical ordering is obvious in both the amorphous La-M and TM-M alloys, the former appear to be more reminiscent of a DRPHS arrangement with very short "pseudonuclei" and considerably less topological ordering as opposed to chemical ordering. It seems quite likely that many different amorphous structures will be necessary to describe the various different amorphous metal alloys such as La-(Al-Ga-Au) and the related TM-M and early transition metal-late transition metal alloys. Input parameters to successful models of these structures will have to include some

reasonable estimation of the interatomic potentials in order to introduce a basis for the chemical ordering in these materials, as well as size ratios, boundary conditions, and other topological parameters.

REFERENCES

1) W. Klement, Jr., R. H. Willens, and Pol Duwez, Nature 187, 869 (1960).

2) Pol Duwez and R. H. Willens, Trans. Met. Soc. AIME 227, 362 (1963).

3) Paul Pietrokowsky, Rev. Sci. Instrum. 34, 445 (1963).

4) H. S. Chen and C. E. Miller, Met. Res. Bull. 11, 49 (1976).

5) H. L. Luo and Pol Duwez, Appl. Phys. Letters 2, 21 (1963).

6) Pol Duwez, R. H. Willens and R. C. Crewdson, J. Appl. Phys. 36, 2267 (1965).

7) T. Ichikawa, Phys. Stat. Sol. (a) 19, 707 (1973).

8) J. Blétry and J. F. Sadoc, J. Phys. F 5, L110 (1975).

9) T. M. Hayes, J. W. Allen, J. Tauc, B. C. Giessen and J. J. Hauser, Phys. Rev. Lett. 40, 1282 (1978).

10) P. Eisenberger and George S. Brown, Solid State Comm. 29, 481 (1979).

11) B. E. Warren, "X-ray Diffraction", Addison-Wesley, Reading, Massachusetts, 1969.

12) B. E. Warren, H. Krutter, and O. Morningstar, J. Amer. Ceram. Soc. 19, 202 (1936).

13) R. Kaplow, S. L. Strong, and B. L. Averbach, in "Local Atomic Arrangements Studied by X-ray Diffraction", (J. B. Cohen and J. E. Hilliard, eds.), pg. 159. Gordon and Breach, New York,1966.

14) C. J. Pings and J. Waser, J. Chem. Phys. 48, 3016 (1968).

15) C. N. J. Wagner, Advan. X-Ray Anal. 12, 50 (1969).

16) B. E. Warren, Progr. Metal Phys. 8, 147 (1959).

17) L. H. Germer and A. H. White, Phys. Rev. 60, 447 (1941).

18) V. H. Tiensuu, S. Ergun, and L. E. Alexander, J. Appl. Phys. 35, 1718 (1964).

19) C. W. B. Grigson and E. Barton, Brit. J. Appl. Phys. 18, 175 (1967).

20) A. Bienenstock and A. S. Posner, Arch. Biochem. Biophys. 124, 604 (1968).

21) C. N. J. Wagner, T. B. Light, N. C. Halder and W. E. Lukens, J. Appl. Phys. 39, 3690 (1968).

22) G. S. Cargill III, J. Appl. Phys. 41, 12 (1970).

23) W. E. Lukens, Ph.D. Thesis, Yale University, New Haven, Connecticut, 1971.

24) J. D. Bernal, Nature (London) 183, 141 (1959).

25) J. D. Bernal, Nature (London) 185, 68 (1960).

26) J. D. Bernal, Proc. Royal Soc., Ser. A 280, 299 (1964).

27) J. L. Finney, Proc. Royal Soc., Ser. A 319, 479 (1970).

28) G. D. Scott and D. M. Kilgour, J. Phys. D. 2, 863 (1969).

29) J. L. Finney, Nature (London) 266, 309 (1977).

30) Charles H. Bennett, J. Appl. Phys. 43, 2727 (1972).

31) G. A. Connell, Solid State Comm. 16, 109 (1975).

32) J. A. Barker, J. L. Finney and M. R. Hoare, Nature (London) 257, 120 (1975).

33) L. von Heimendahl, J. Phys. (F) 5, L141 (1975).

34) D. E. Polk, Scr. Metall. 4, 117 (1970).

35) G. S. Cargill III and R. W. Cochrane, J. Phys. (Paris) 35, C4-269 (1974).

36) D. E. Polk, Acta Met. 20, 485 (1972).

37) Y. Hiwatari, H. Matsuda, T. Igita, and A. Ueda, Prog. Theor. Phys. 52, 1105 (1974).

38) A. Rahman, M. J. Mandell and J. McTague, J. Chem. Phys. 64, 1564 (1976).

39) W. B. Streett, J. H. Raveche and R. D. Mountain, J. Chem. Phys. 61, 1960 (1974).

40) G. S. Cargill III, Solid State Physics 30, 227 (1975).

41) J. E. Enderby, D. M. North and P. A. Egelstaff, Phil. Mag. 14, 961 (1966).

42) J. F. Sadoc and J. Dixmier, Mat. Sci. and Eng. 23, 187 (1976).

43) T. Mizoguchi, T. Kudo, T. Irisawa, N. Watanabe, N. Niimura, M. Misawa, and K. Suzuki, Proc. 3rd Int. Conf. Rapidly Quenched Metals 2, 384 (1978).

44) Y. Waseda and H. S. Chen, Proc. 3rd Int. Conf. Rapidly Quenched Metals 2, 415 (1978).

45) P. Fuoss, Ph.D. Thesis, Stanford University, Palo Alto, California, 1980.

46) D. R. Chipman, L. D. Jennings, and B. C. Giessen, presented at the Topical Conf. on Atomic Scale Structure of Amorphous Solids, Yorktown Heights, N.Y. 3-5 April, 1978.

47) G. S. Cargill III and C. C. Tsuei, Proc. 3rd Int. Conf. Rapidly Quenched Metals 2, 337 (1978).

48) W. L. Johnson, S. J. Poon, J. Durand, and P. Duwez, Phys. Rev. B 18, 206 (1978).

49) W. L. Johnson and A. R. Williams, Phys. Rev. B 20, 1640 (1979).

50) A. R. Williams and W. L. Johnson, J. Non-Cryst. Solids 34, 121 (1979).

51) H. Berman, Am. Mineralogist 24, 434 (1939).

52) G. Breit, Phys. Rev. 27, 362 (1926).

53) N. S. Gingrich, Rev. Mod. Phys. 15, 90 (1943).

54) Don T. Cromer and J. T. Waber, Acta Cryst. 18, 104 (1965).

55) Don T. Cromer and Joseph B. Mann, J. Chem. Phys. 47, 1892 (1967).

56) Don T. Cromer, J. Chem. Phys. 50, 4857 (1969).

57) Don T. Cromer, Acta Cryst. 18, 17 (1965).

58) Rodney P. Elliot, "Constitution of Binary Alloys, First Supplement", McGraw-Hill Book Company, USA, 1965.

59) W. B. Pearson, "A Handbook of Lattice Spacings and Structures of Metals and Alloys", Pergamon Press Ltd., London, 1967.

60) K. Andres, Phys. Rev. 168, 708 (1968).

61) K. Schwidtal, Z. Physik 169, 569 (1962).

62) T. F. Smith and H. L. Luo, J. Phys. Chem. Solids 28, 569 (1967).

63) J. Wittig, C. Probst, and W. Wiedemann, in "Low Temperature Physics LT-13, Superconductivity", (K. D. Timmerhaus, W. J. O'Sullivan, and E. F. Hammel, eds.), Vol. 3, pg. 491, Plenum Press, New York, 1974.

64) W. L. Johnson, S. J. Poon, and P. Duwez, Phys. Rev. B 11, 150 (1975).

65) K. Agyeman, R. Müller, and C. C. Tsuei, Phys. Rev. B 19, 193 (1979).

66) P. M. Nast, K. Samwer, and G. V. Minnigerode, Z. Physik B 38, 89 (1980).

67) W. H. Schull, D. G. Naugle, S. J. Poon, and W. L. Johnson, Phys. Rev. B 18, 3263 (1978).

68) A. Williams, unpublished results.

69) J. Logan, Scr. Metall. 9, 379 (1975).

70) J. H. Konnert and J. Karle, Acta Cryst. A 29, 702 (1973).

71) J. F. Sadoc and J. Dixmier, in "The Structure of Non-Crystalline Materials", (P. H. Gaskell, ed.), pg. 85, Taylor and Francis, London, 1977.

72) D. S. Boudreaux and J. M. Gregor, J. Appl. Phys. 48, 152 (1977).

73) Takeo Fujiwara and Yasushi Ishii, J. Phys. F 10, 1901 (1980).